frontiers in Materials

ORIGINAL RESEARCH
published: 16 February 2022
doi: 10.3389/fmats.2022.843438

# Novel Natural Surfactant-Based Fatty Acids and Their Corrosion-Inhibitive Characteristics for Carbon Steel-Induced Sweet Corrosion: Detailed Practical and Computational Explorations

*Hany M. Abd El-Lateef[1,2]*, Hossam S. El-Beltagi[3,4], Maged Elsayed Mohamed Mohamed[5,6], Mahmoud Kandeel[7,8], Esam Bakir[1,9], Arafat Toghan[10,11], Kamal Shalabi[12], Ahmed H. Tantawy[13] and Mai M. Khalaf[1,2]*

[1]Department of Chemistry, College of Science, King Faisal University, Al-Ahsa, Saudi Arabia, [2]Department of Chemistry, Faculty of Science, Sohag University, Sohag, Egypt, [3]Agricultural Biotechnology Department, College of Agriculture and Food Sciences, King Faisal University, Al-Ahsa, Saudi Arabia, [4]Biochemistry Department, Faculty of Agriculture, Cairo University, Giza, Egypt, [5]Department of Pharmaceutical Sciences, College of Clinical Pharmacy, King Faisal University, Al-Ahsa, Saudi Arabia, [6]Department of Pharmacognosy, College of Pharmacy, Zagazig University, Zagazig, Egypt, [7]Department of Biomedical Sciences, College of Veterinary Medicine, King Faisal University, Al-Ahsa, Saudi Arabia, [8]Department of Pharmacology, Faculty of Veterinary Medicine, Kafrelsheikh University, Kafrelsheikh, Egypt, [9]Department of Chemistry, Faculty of Science, Ain Shams University, Cairo, Egypt, [10]Chemistry Department, Faculty of Science, South Valley University, Qena, Egypt, [11]Chemistry Department, College of Science, Imam Mohammad Ibn Saud Islamic University (IMSIU), Riyadh, Saudi Arabia, [12]Chemistry Department, Faculty of Science, Mansoura University, Mansoura, Egypt, [13]Chemistry Department, Faculty of Science, Benha University, Benha, Egypt

OPEN ACCESS

**Edited by:**
Lei Guo,
Tongren University, China

**Reviewed by:**
Rachid Hsissou,
Ibn Tofail University, Morocco
Tengfei Xiang,
Anhui University of Technology, China
Renhui Zhang,
East China Jiaotong University, China

***Correspondence:**
Hany M. Abd El-Lateef
hmahmed@kfu.edu.sa

**Specialty section:**
This article was submitted to Environmental Degradation of Materials, a section of the journal Frontiers in Materials

**Received:** 25 December 2021
**Accepted:** 12 January 2022
**Published:** 16 February 2022

**Citation:**
Abd El-Lateef HM, El-Beltagi HS, Mohamed Mohamed ME, Kandeel M, Bakir E, Toghan A, Shalabi K, Tantawy AH and Khalaf MM (2022) Novel Natural Surfactant-Based Fatty Acids and Their Corrosion-Inhibitive Characteristics for Carbon Steel-Induced Sweet Corrosion: Detailed Practical and Computational Explorations. Front. Mater. 9:843438. doi: 10.3389/fmats.2022.843438

Steel alloys are significant industrial substances, but they generally suffer severe corrosion under harsh conditions. Using inhibitors is an efficacious method to impede corrosion. So, in this study, two novel natural surfactants based on soybean oil have been synthesized by a facile route, namely, 1-(bis(2-hydroxyethyl)amino)-1-oxooctadecan-9-yl sulfate 2-hydroxyethan-1-aminium (CSM) and–N-$(C_2H_4\text{-}OH)_2$; 1-(bis(2-hydroxyethyl)amino)-1-oxooctadecan-9-yl sulfate bis(2-hydroxyethyl)aminium (CSD), and their chemical structures were elucidated by physical–chemical approaches, Fourier transform infrared (FT-IR) spectroscopy, and surface activity measurements. The inhibitive effect of natural surfactants (CSM and CSD) on the C-steel corrosion in $CO_2$-saturated 3.5% NaCl has been estimated in this investigation by electrochemical and surface analyses including electrochemical impedance spectroscopy (EIS), potentiodynamic polarization (PDP), linear polarization resistance (LPR) corrosion rate, X-ray photoelectron spectroscopy (XPS), and field-emission scanning electron microscope/energy-dispersive X-ray spectroscopy (FESEM/EDX) approaches. The EIS study reveals the value of $R_p$ augmented to an increase of 913.5 $\Omega\,cm^2$ with a protection capacity of 96.1% at 150 ppm (CSD). The outcomes of PDP suggested that CSM and CSD are mixed-type inhibitors. XPS and FESEM/EDX analyses determined the protective film formation on a metal interface having undamaged surface morphology and more homogeneities in the occurrence of the surfactant. Moreover, the adsorption of natural surfactants on the metal substrate takes place based on the model of Langmuir isotherm. Density functional theory

(DFT) calculations and Monte Carlo (MC) simulations were selected for attaining basic atomic/electronic-scale details about the prepared surfactants, which support the practical findings. This study is intended to investigate the protection of C-steel using sweet service conditions with green extract surfactants.

**Keywords: green extract surfactants, sweet corrosion, DFT calculations, corrosion protection, FESEM/ EDX**

## INTRODUCTION

Sweet corrosion (carbon dioxide corrosion) has gained abundant attention in the gas and oil industry, processing, and transportation. It is because of the common practice of using carbon dioxide-saturated $H_2O$ in oil wells to diminish pumped fluid viscosity and improve oil recovery. A significant phenomenon is that when carbon dioxide dissolves in $H_2O$, $H_2CO_3$ (carbonic acid) is formed which is more corrosive than HCl solution under similar conditions (Ramírez-Estrada et al., 2017). $CO_2$ corrosion differs significantly depending on the alteration in the environmental conditions (Liu et al., 2009; Hua et al., 2015; Juárez et al., 2018; Li et al., 2019). The $CO_2$ corrosion mechanism and its effects, including the water/gas mixture temperature, were investigated by many scientists (Singh et al., 2015; Chen et al., 2017; Olajire, 2017).

Alloys of carbon steel are the most commonly used manufacturing materials for pipelines in petroleum manufacturing. However, they are very vulnerable to corrosion under sweet corrosion environments. In order to enhance their performance, corrosion inhibitors are commonly applied. Nevertheless, a deep understanding of the action mechanism of the corrosion mitigation route is still required for reliable implementations (Hsissou et al., 2019a; Saleh et al., 2019; Hsissou et al., 2020a; Zhang et al., 2021a).

Inhibitor molecules are the compounds that diminish or inhibit corrosion if they are introduced at low doses in a corrosive solution. The efficiency of organic inhibitors depends on their rates of adsorption and covering competencies on the steel interface (Nesõić, 2007; Hsissou et al., 2019b). Numerous authors have stated that the adsorption of the organic inhibitor is generally attributed to the molecular construction, electrolyte type, and metal surface charge (Hsissou and Elharfi, 2020; Zhang et al., 2021b; Yang et al., 2021; Zhu et al., 2021). It is well recognized that the existence of hydrophobic and hydrophilic groups in the inhibitor structure favors the adsorption route at the interface of metal/solution (Migahed et al., 2014). Therefore, the use of predictable surfactants consisting of one hydrophobic chain and one hydrophilic head group as corrosion additives has been extensively investigated. It was observed that these amphiphilic molecules can adsorb on the steel interface to provide a defensive film and have a noticeable protecting efficacy close to their critical micellar concentration (CMC) (García et al., 1999). Fatty acid salts have found application as corrosion additives for steel in different aggressive environments (Abd El-Lateef and Tantawy, 2016; Shalabi and AhmedNazeer, 2019; Abd El-Lateef et al., 2020). Their low solubility and formation of insoluble soaps in hard $H_2O$ make them hard to use. To remove this difficulty and enhance their service characteristics, fatty acids are adapted, for example, by sulfating or by adding new groups in their structure, to increase solubility. Therefore, this study aims to identify and produce efficient inhibitors for the protection of steel pipelines from corrosion under sweet conditions.

Recently, natural surfactants were extensively used in diverse manufacturing applications owing to their distinctive properties such as great viscosity, enhancement of wetting, outstanding adsorption feature, solubilization capacity, and antimicrobial accomplishments (Tantawy et al., 2020). The N atom ($-N^+-$) quaternary group of natural surfactants is demarcated to be significant for a number of important parameters such as antistatic characteristics, and adsorption onto the negative charge of solid surfaces (García et al., 1999).

Herein, novel natural surfactants containing fatty acid salts were extracted using soybean oil as they are more soluble and possess improved inhibitive features. Soybean oil is gaining increased attention due to its characteristics such as comparatively low price and availability (Clemente and Cahoon, 2009). Two kinds of natural surfactants as green, safe, and environmentally friendly inhibitors were investigated for the corrosion of C-steel in sweet conditions (carbon dioxide-saturated 3.5% sodium chloride solution) using EIS, PDP, and LPR corrosion approaches. XPS and FESEM/EDX methods were utilized to inspect the alteration in the metal surfaces corroded in the uninhibited and inhibited systems. The computational analysis of the prepared surfactants was carried out using DFT calculations and MC simulations in order to confirm the experimental findings.

## EXPERIMENTAL PART

### Chemical Structure of C-Steel Grade 080A15

C-steel substrates with an area of 1.0 $cm^2$ and subsequent elemental structure silicon, 0.16%; nickel, 0.01%, chromium, 0.02%; sulfur, 0.02%; phosphorous, 0.01%; carbon, 0.16%; manganese, 0.68%; and remaining Fe were used for corrosion measurements.

### Surfactant Preparation

Soybean oil was hydrolyzed with 20% sodium hydroxide solution for 8 h at a temperature of 85–90°C. This method produced sodium salts of fatty acids with good yield (87%). Then, the sodium salts of fatty acids were reacted with concentrated hydrochloric acid solution (37%) for extracting the fatty acids. The sulfating processes were performed on the extracted fatty acids. The product is a sulfated fatty acid with good yield (81%).

The products were characterized by physical–chemical approaches and FT-IR spectroscopy.

The sulfated fatty acids were reacted with the equimolar ratio from 10% mono- and diethanolamine at 25°C to yield mono- and diethanolamine salts by the following structures: [R-CH-($SO_3$OX)-COOX] (where $X$ = –NH-$C_2H_4$-OH; 1-[bis(2-hydroxyethyl) amino]-1-oxooctadecan-9-yl sulfate 2-hydoxyethan-1-aminium (**CSM**) and –N-($C_2H_4$-OH)$_2$; and 1-[bis(2-hydroxyethyl)amino]-1-oxooctadecan-9-yl sulfate bis[2-hyroxyethyl)aminium (**CSD**)].

## Instrumentation

The chemical construction of the extracted natural surfactants was clarified *via* melting points (Gallen–Kamp); FT-IR spectroscopy was performed in KBr (NICOLET 5700 FT-IR). In addition, the K6 processor-Tensiometer (KRÜSS-Company, Germany) using the ring technique was used to determine the surface tension of synthesized surfactants in 3.5% sodium chloride solution at 25°C.

## Corrosive Medium

The corrosive medium, 3.5% sodium chloride, was prepared by dissolving analytical grade sodium chloride in double-distilled $H_2O$. Before experimentation, the prepared 3.5% sodium chloride was stirred for 40 min in 500 ml cells. Then, the cells were retained for 50 min under a pressure of 0.9 bars in a heater at 323 K. The NaCl medium was saturated with $CO_2$. The concentration range of the synthesized additives was from 10 to 150 mg $L^{-1}$ used for corrosion inhibition experiments.

## Corrosion Inhibition Performance

Corrosion experiments were completed in 3.5% brine solution saturated with carbon dioxide with different doses of the prepared natural surfactants. The Gamry Potentiostat/Galvanostat/ZRA device was used for the electrochemical experiments using 3-electrode cell systems, in which Pt-sheet assisted as a counter electrode, saturated silver/silver chloride ($Ag/AgCl_{(sat)}$) served as the reference electrode, and C1018-steel was the working electrode (WE). Before all electrochemical measurements, the WE was retained in the corrosive medium for 30 min to reach constant OCP values. The PDP experiments were performed in a potential range of −0.4–1.0 V vs. $E_{OCP}$ at a sweep rate of 0.2 mV $s^{-1}$. EIS was accomplished at $E_{OCP}$ using a 10 mV peak-to-peak voltage excitation in a frequency range of 100 kHz–0.1 Hz. Different parameters were attained from the plot simulations using Gamry Echem Analyst software. All the experimentations were carried out twice, and the value averages were recorded using the best figures. The LPR corrosion rate measurements were completed as discussed previously in Abd El-Lateef (2020).

## Computational Details

Full optimization of the two inhibitor molecules CSM and CSD was studied using DFT calculations with B3LYP-functional (Saha et al., 2015; Singh et al., 2016) and basis set 6–31g (d,p) implemented in the Dmol3 module in Materials Studio V. 7.0 program (Haque et al., 2017; Singh et al., 2018a; Singh et al., 2018b). The results obtained from the simulation, for instance, the lowest unoccupied molecular orbital (LUMO), the highest occupied molecular orbital (HOMO), gap energy ($\Delta E$), electronegativity ($\chi$), hardness ($\eta$), global softness ($\sigma$), dipole moment ($\mu$), electrophilicity index ($\omega$), and number of electrons transferred ($\Delta N$) were investigated. The electronegativity, global softness, hardness, electrophilicity index, and number of electrons transferred were calculated as follows:

$$\chi = \frac{-E_{HOMO} - E_{LUMO}}{2}, \tag{1}$$

$$\eta = \frac{1}{\sigma} = \frac{E_{LUMO} - E_{HOMO}}{2}, \tag{2}$$

$$\omega = \frac{\chi^2}{2\eta}, \tag{3}$$

$$\Delta N = \frac{\phi - \chi_{inh}}{2\left(\eta_{Fe} - \eta_{inh}\right)}, \tag{4}$$

where $\varphi$ is function work of Fe(110), $\chi_{inh}$ represents the inhibitor electronegativity, and $\eta_{Fe}$ and $\eta_{inh}$ are the chemical hardness of Fe (0 eV) and the inhibitor, respectively.

For MC simulations, the suitable adsorption configurations of the CSM and CSD molecules on the Fe(110) surface were discovered by using the adsorption locator module in the Materials Studio V. 7.0 program (Abd El-Lateef et al., 2020). Initially, the adsorbate molecules had been optimized in the operating COMPASS force field. Then, in a simulation box (37.24 × 37.24 × 59.81 Å), adsorption of the CSM and CSD, $Cl^-$ ions, hydronium ions, and water molecules with surface of Fe(110) was accomplished (Tantawy et al., 2020).

## Surface Characterization by XPS, EDX, and FESEM

In order to inspect the modifications in surface topologies of the C-steel specimens after corrosion experiments, the samples were first immersed in the corrosive solution with and without synthetic surfactants for 20 h, then cleaned with double-distilled $H_2O$ and acetone, and desiccated with cool air. The surface morphology of the investigated specimens was detected by EDX complemented with a FESEM. An XPS study was performed as mentioned in our previous study (Abd El-Lateef et al., 2020). The investigated specimens attained from LPR corrosion were utilized in examinations.

# RESULTS AND DISCUSSIONS

## Chemical Configuration of the Prepared Natural Surfactants

The structural features of purified compounds of the extracted fatty acids were established by FT-IR investigation as presented in **Supplementary Table S1**; **Supplementary Figure S1** (Supporting data). The fatty acid peaks are in agreement with the distinctive peaks described previously (Shapaval et al., 2014). The peak at ≈ 1706 $cm^{-1}$ is related

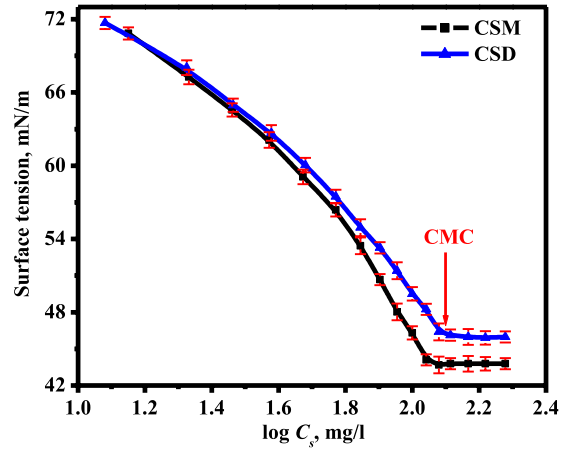


**FIGURE 1 |** Variation of surface tension ($\gamma$) vs. surfactant concentration in 3.5% NaCl solution.

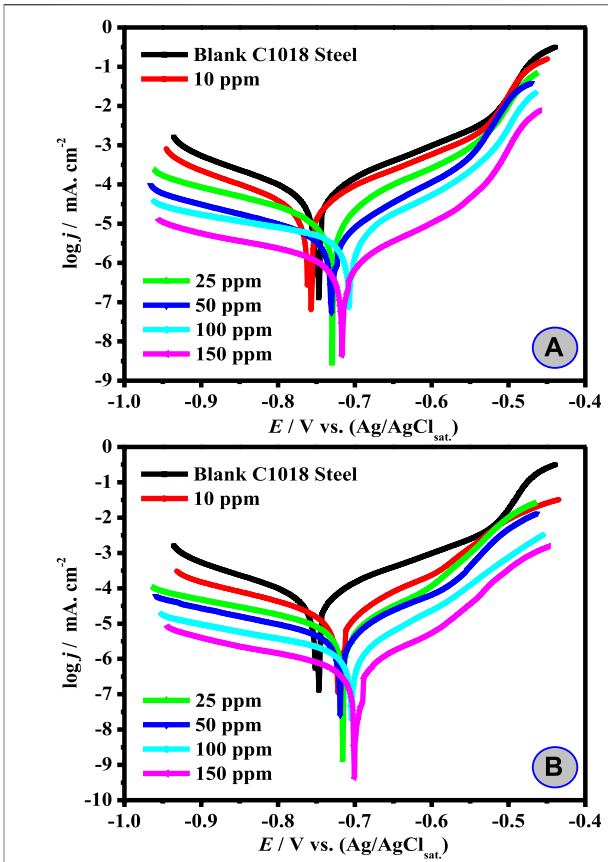


**FIGURE 2 |** Tafel plots for C1018-steel 3.5% NaCl saturated $CO_2$ solution without and with different concentrations of **(A)** CSM and **(B)** CSD at 50 ± 1°C.

to the carbonyl group (C=O) of the –COOH group; however, the band at 1,488 $cm^{-1}$ is attributed to –C=C–. This –C=C– bond was damaged after the practicability of sulfating. The peak at 1,359 $cm^{-1}$ is owing to the stretching absorption band S–O. It designates the whole abstraction of the –C=C– bond by adding practicability.

The physico-chemical characteristics of the extracted fatty acids before and after the sulfating process were examined. The results exhibited that the acid number augmented was from 134.7 (before sulfating process) to 278.4 (after the sulfating process) and no interaction with iodine was determined after the sulfating process. These outcomes also established the whole elimination of the C=C bond by sulfuric acid addition and production of sulfated fatty acid.

## Surface Activity Measurements

The concentration of critical micelle concentration (CMC) values of the synthesized natural surfactants was estimated by plotting the change in the surface tension ($\gamma$) against their concentrations in mg/l in 3.5% NaCl solution at 25°C (**Figure 1**). The CMC values were found to be 123.1 and 102.3 for CSM and CSD, respectively. Accordingly, the CMC value of the synthesized natural surfactant is declined by increasing the hydrophobic chain length; this could be related to decreasing the solubility and increasing hydrophobicity of the synthesized natural surfactant, that is, by increasing the hydrophobic chain length, the tendency of the surfactant molecule to form a micelle is consequently reduced by CMC (Abd El-Lateef et al., 2020).

The surface-active parameters such as effectiveness ($\Pi_{cmc}$), the surface area ($A_{min}$), and efficacy of interfacial adsorption ($\Gamma_{max}$) were calculated based on surface tension measurement. The effectiveness ($\Pi_{cmc}$) values indicated that the most active surfactant is CSD, which provides the largest decline in the surface tension at the CMC. Moreover, the $\Gamma_{max}$ and $A_{min}$ values exhibited that the increase in the length of a hydrophobic chain of the surfactant shifts $\Gamma_{max}$ to lesser concentration values and $A_{min}$ is increased owing to the increasing hydrophobic chain of the area occupied by each surfactant molecule increase.

According to Gibb's adsorption equations, the thermodynamic parameters of micellization ($\Delta G^0_{mic}$) and adsorption ($\Delta G^0_{ads}$) of the prepared natural surfactants were determined. The values of $\Delta G^0_{mic}$ and $\Delta G^0_{ads}$ ($\Delta G^0_{mic}$ = -23.25 and -23.78 kJ $g^1$ and $\Delta G^0_{ads}$ = -25.12 and -25.46 kJ $g^1$ for CSM and CSD, respectively) are continuously negative, leading to the spontaneity of adsorption and micellization processes, but there are more upsurges in the negativity value of $\Delta G^0_{ads}$ than $\Delta G^0_{mic}$, demonstrating the inclination of the surfactant compounds to be adsorbed at the metal/electrolyte surface (Tantawy et al., 2020). Moreover, $\Delta G^0_{ads}$ values increase by increasing the hydrophobic chain, signifying that the inclination of the surfactant molecules to be absorbed on the interface follows the order CSD > CSM.

## Tafel Extrapolation Method (Effect of Inhibitor Concentration and Temperature)

The impact of the natural surfactant (CSM and CSD) dose on the Tafel anodic and cathodic polarization profiles of C-steel in 3.5%

**TABLE 1 |** Tafel parameters and inhibition efficiency of C-steel in 3.5% NaCl saturated with $CO_2$ in the absence and presence of diverse doses of the prepared surfactants at 50 ± 1°C.

| Inhibitor code | $C_{inh}$/mg $L^{-1}$ | $j_{cor}$ ±SD/μAcm$^{-2}$ | -$E_{cor}$/V (SCE) | $\beta_a$/V dec $^{-1}$ | -$\beta_c$/V dec $^{-1}$ | $\theta$ | $\eta_T$/% |
|---|---|---|---|---|---|---|---|
| Blank | 0.0 | 1045.1 ± 38 | 0.746 | 0.073 | 0.146 | -- | -- |
| CSM | 10 | 567.4 ± 31 | 0.756 | 0.084 | 0.166 | 0.457 | 45.7 |
| | 25 | 390.8 ± 24 | 0.728 | 0.089 | 0.162 | 0.626 | 62.6 |
| | 50 | 246.6 ± 15 | 0.730 | 0.086 | 0.157 | 0.764 | 76.4 |
| | 100 | 115.9 ± 9 | 0.708 | 0.076 | 0.158 | 0.889 | 88.9 |
| | 150 | 25.1 ± 2.1 | 0.715 | 0.079 | 0.161 | 0.976 | 97.6 |
| CSD | 10 | 497.4 ± 26 | 0.718 | 0.086 | 0.162 | 0.524 | 52.4 |
| | 25 | 312.4 ± 21 | 0.714 | 0.083 | 0.165 | 0.701 | 70.1 |
| | 50 | 148.3 ± 17 | 0.719 | 0.088 | 0.163 | 0.858 | 85.8 |
| | 100 | 71.1 ± 5 | 0.701 | 0.085 | 0.160 | 0.932 | 93.2 |
| | 150 | 14.6 ± 1.1 | 0.698 | 0.079 | 0.168 | 0.986 | 98.6 |

brine solution saturated with carbon dioxide at a sweep rate 0.2 mV $s^{-1}$ and 323 K is presented in **Figure 2** A, B. Corrosion parameters were computed based on the anodic and cathodic potential vs. current density features in the potential of Tafel area (Hsissou et al., 2020b). The corrosion current density values (*j*cor) for the titled C1018-steel lacking and with the surfactant, respectively, were estimated by the anodic and cathodic extrapolation of Tafel lines to the corrosion potential (*E*cor). It could be appreciated that the occurrence of surfactant additive results is a noticeable modification in both anodic and cathodic divisions of the polarization plots in the direction of *j*cor. It is worth noting that the surfactants affect the mutually anodic and cathodic processes. The surfactant additive might decline the corrosion rate by the lessening of C1018-steel reactivity. Based on this phenomenon, a decline of both the cathodic and anodic reactions arises from the surfactant adsorption on the conforming efficient centers (Alnajjar et al., 2022). The protection efficacy ($\eta_T$/%) in the occurrence of CSM for CSD was intended from the corrosion current density in the blank ($j^0_{cor}$) and inhibited ($j^s_{cor}$) systems by the following equation. (The values are recorded in **Table 1**):

$$\eta_T/\% = \left[\frac{j^0_{cor} - j^s_{cor}}{j^0_{cor}}\right] \times 100 = \theta \times 100. \quad (5)$$

The outcomes in **Table 1** revealed that *j*cor declines and $\eta_T$/% upsurges as the surfactant dose is augmented. These findings indicated that hindrance of the electrode reactions takes place at mutually anodic and cathodic locations as a consequence of coverage of these places by CSM and CSD species. The maximum value of $\eta_T$/% (98.6%) was attained for the maximum dose (150 ppm) CSD in the investigated corrosive media. This might be ascribed to the increase in active position number, molecular size, and electron densities (Hsissou et al., 2021a). The increase in $\eta_T$/% with growing the [surfactant] could be inferred based on the adsorption quantity, and part of the covered surface increased with increasing additive concentration (Ansari et al., 2014). The *E*cor values of both CSM and CSD additives showed a slight shift toward both anodic and cathodic directions (the differences in *E*cor are lower ±85 mV) and did not demonstrate any definite trend in $CO_2$-saturated NaCl solution. Such findings proposed that the CSM and CSD natural surfactants can be classified as mixed-type corrosion inhibitors, that is, both the hydrogen evolution reaction and the anodic Fe dissolution were blocked (Bentiss et al., 2005).

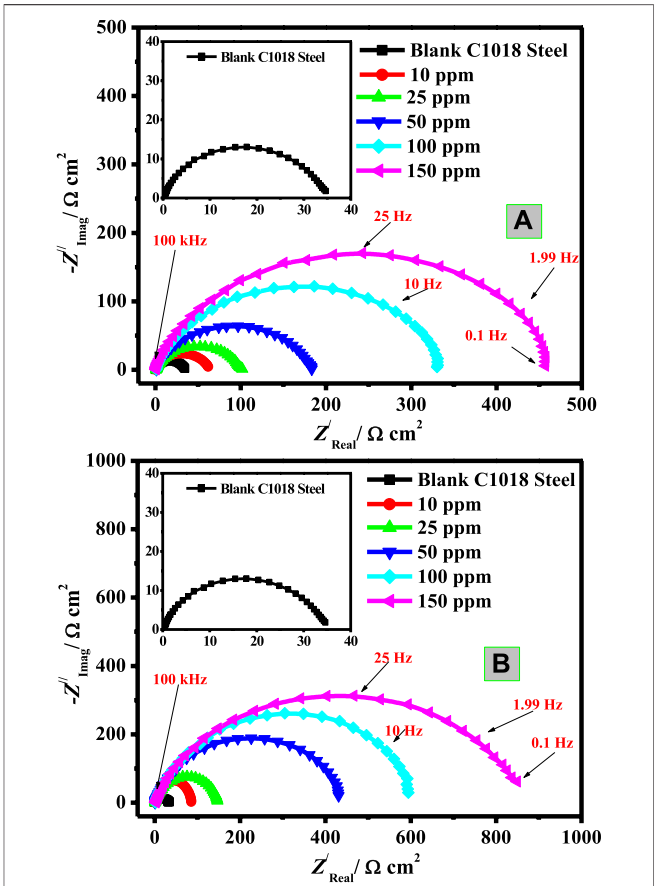


**FIGURE 3 |** Nyquist plots of C-steel/$CO_2$-saturated 3.5% NaCl/surfactant uninhibited and inhibited by diverse concentration of **(A)** CSM and **(B)** CSD at 50 ± 1°C.

From **Table 1**, it is correspondingly detected that the cathodic ($\beta$c) and anodic ($\beta$a) Tafel slopes of the protected corrosive medium do not follow a definite array with an upsurge in

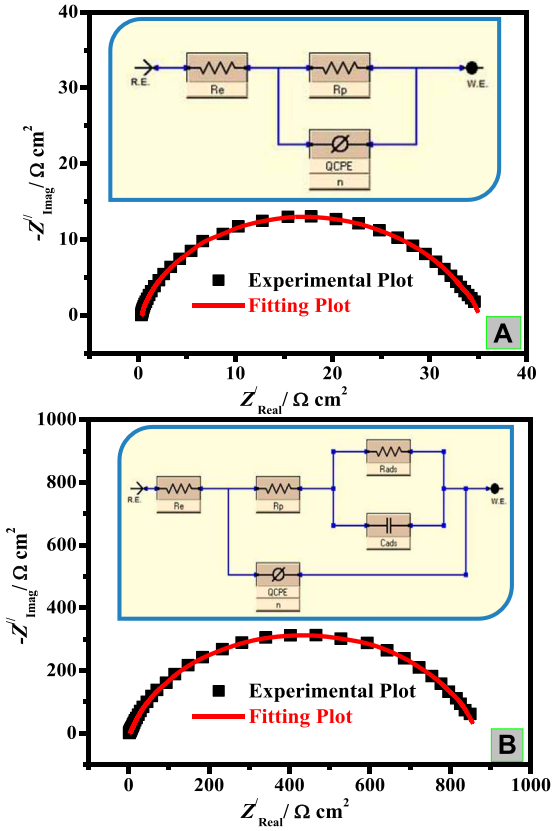


**FIGURE 4 |** Comparison of experimental Nyquist and Bode phase data (points) and fitted data (line) measured for C-steel in blank **(A)** and inhibited systems **(B)**. Inset: EEC for C-steel/$CO_2$-saturated 3.5% NaCl/surfactant uninhibited **(A)** and inhibited **(B)** systems.

surfactant dose. These outcomes designate that these natural surfactants act by merely hindering the obtainable surface area. The high part of the covered surface $\theta$ value close to unity designates nearly a complete coverage of the electrode surface with the adsorbed surfactant additives. The protection capacity of the synthesized natural surfactants was augmented in the subsequent order: CSM < CSD. High electron density and higher surfactant size on the adsorption sites might be accountable for high protection efficacy.

The effect of temperature for the deterioration of C-steel in blank and inhibited test solution was studied. To obtain more knowledge about the adsorption type of the extracted natural surfactants at different temperatures, the Tafel polarization method was performed at 303–333 K. The adsorption mechanism (physically or chemically onto the metal surface) could be proposed from the consideration of these findings. The change in $j_{cor}$ and $\eta_T$/%) with temperature in the uninhibited and inhibited systems is presented in **Supplementary Figure S2**. It could be seen that $j_{cor}$ increases with temperature for C-steel in the blank corrosive medium (**Supplementary Figure S2A**). In the presence of CSM and CSD surfactants, $j_{cor}$ is smaller than that in blank solution. These results indicate that the CSM and CSD surfactants are effective at the studied temperature range. The effect of temperatures on the inhibition capacity of C-steel in the corrosive medium containing CSM and CSD surfactants is presented in **Supplementary Figure S2B**. Based on this plot, inhibition efficiency increases by increasing the reaction temperature. This performance is characteristic of a chemisorption mechanism (Tantawy et al., 2020).

## EIS Investigations

To further assess the corrosion inhibition action of the synthesized natural surfactants on C-steel corrosion in blank and inhibited systems, EIS experiments were carried out. The blank and protected C-steel samples display a sole capacitive loop which designates that metal corrosion in the current corrosive medium (3.5% NaCl-saturated with carbon dioxide) includes a charge transfer mechanism (Soltani et al., 2016). Examination of **Figure 3A**, B exhibited that Nyquist profile diameters increase with increasing concentrations of the two natural surfactants (CSM and CSD), which is ascribed to their augmented adsorption on the interfaces of steel/corrosive solution (Kowsari et al., 2014).

Comparison of experimental Nyquist data (points) and fitted data (line) measured for C-steel in the blank (A) and inhibited systems (B) is presented in **Figure 4**. The EIS parameters were computed with the assistance of a suitable equivalent circuit (EEC) presented in **Figures 4A,B** (inset) and are recorded in **Table 2**. This EEC includes $R_e$ (electrolyte resistance), $R_p$ [resistance of polarization; $R_p = R_{dl}$ (diffuse layer resistance) + $R_{ct}$ (charge transfer resistance) + $R_a$ (other collected resistance)], and CPE (constant phase element), which is utilized instead of pure capacitance to recompense the inhomogeneity of the surface (Yilmaz et al., 2016), arising owing to impurities, dislocations, roughness of surface, grain boundaries fractality, and active center distribution (Ortega-Toledo et al., 2011). In the case of the inhibited medium (**Figure 4B**), CPE is in sequences to the parallel of capacitance as $C_{ads}$ due to the surfactant adsorption layer and the resistance attributed to inhibitor adsorption ($R_{ads}$). The CPE impedance ($Z_{CPE}$) is assumed by the subsequent equation (Musa et al., 2011):

$$Z_{CPE} = \frac{1}{Y_0 (j\omega)^n}, \tag{6}$$

where $j$ represents an imaginary number ($j = \sqrt{-1}$), $Y_o$ characterizes the CPE constant, $\omega$ symbolizes the angular frequency, and $n$ is the phase shift factor. The $n$ values = 1, 0.5, 0, and −1 signify pure capacitivity, Warburg impedance resistivity, and inductivity, respectively. The $C_{dl}$ values (double-layer capacitance) were intended from the frequency at the imaginary part of the maximum impedance ($\omega_{max}$) by the following equation (Desimone et al., 2011):

$$C_{dl} = Y_0 (\omega_{max})^{n-1}. \tag{7}$$

The $R_e$ value recorded in **Table 2** is higher for the solution containing CSM and CSD inhibitors than the uninhibited medium. This is ascribed to a decline in the conductivity of electrolytes by the insertion of the instigated surfactants. The outcomes of **Table 2** demonstrated that the $R_p$ values improved on augmenting the surfactant dose, which attributed to larger

**TABLE 2 |** EIS parameters and inhibition efficiency of C-steel in 3.5% NaCl saturated with $CO_2$ in the absence and presence of diverse doses of the prepared surfactants at 50 ± 1°C.

| Inhibitor code | $C_s$/ ppm | $R_s$/ Ω cm$^2$ | $Z_{CPE}$ | | $C_{dl}$/μF cm$^{-2}$ | $R_p$/Ω cm$^2$ | $\theta$ | $\eta_E$/ % |
|---|---|---|---|---|---|---|---|---|
| | | | $Y_0$/ μΩ$^{-1}$ s$^n$ cm$^{-2}$ | $n$ | | | | |
| Blank | 0.0 | 0.24 | 89.88 | 0.731 | 35.2 ± 2.5 | 197.70 | | — |
| CSM | 10 | 0.36 | 51.29 | 0.881 | 61.6 ± 4.4 | 121.78 | 0.428 | 42.8 |
| | 25 | 0.42 | 44.34 | 0.879 | 102.2 ± 7.9 | 87.91 | 0.655 | 65.5 |
| | 50 | 0.46 | 31.22 | 0.861 | 180.6 ± 12.4 | 66.06 | 0.805 | 80.5 |
| | 100 | 0.52 | 23.78 | 0.882 | 354.7 ± 17.6 | 57.165 | 0.901 | 90.1 |
| | 150 | 0.68 | 18.02 | 0.883 | 478.9 ± 21.2 | 31.71 | 0.926 | 92.6 |
| CSD | 10 | 0.72 | 44.49 | 0.875 | 89.1 ± 7.2 | 96.76 | 0.605 | 60.5 |
| | 25 | 0.95 | 38.24 | 0.886 | 164.4 ± 13.1 | 79.29 | 0.785 | 78.5 |
| | 50 | 1.08 | 27.47 | 0.878 | 460.1 ± 29.6 | 61.23 | 0.923 | 92.3 |
| | 100 | 1.22 | 20.51 | 0.908 | 592.8 ± 37.4 | 50.94 | 0.941 | 94.1 |
| | 150 | 1.48 | 15.78 | 0.902 | 913.5 ± 53.6 | 23.42 | 0.961 | 96.1 |

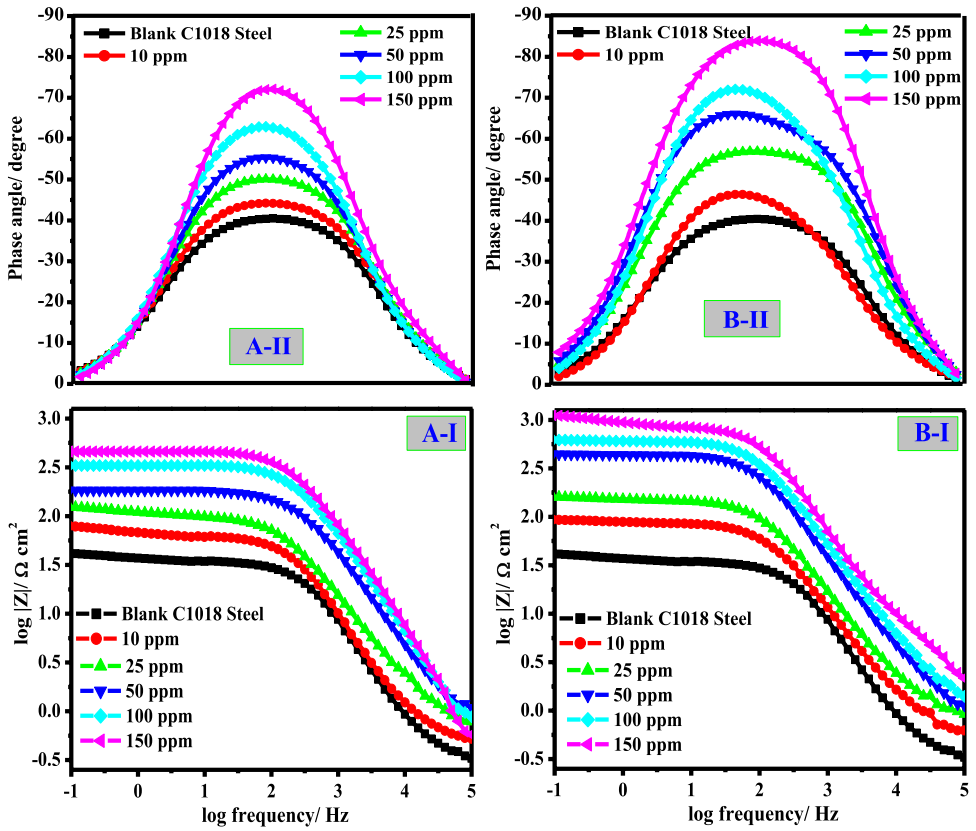


**FIGURE 5 |** Bode **(I)** and Bode phase **(II)** modules of C-steel/$CO_2$-saturated 3.5% NaCl/surfactant uninhibited and inhibited by diverse concentration of **(A)** CSM and **(B)** CSD at 50 ± 1°C.

hindering of the efficient part at the steel surface owing to CSM and CSD adsorption onto the C-steel surface and the disarticulation of the adsorbed $H_2O$ molecules from the metal interface. The values of $n$ are generally relative to the metal surface heterogeneity/homogeneity. As possibly detected, the $n$ value is small for the uninhibited medium, which openly clarifies the great coverage of iron hydroxide/oxide on the Fe bar. Nevertheless, after insertion, the quantities of CSM and CSD

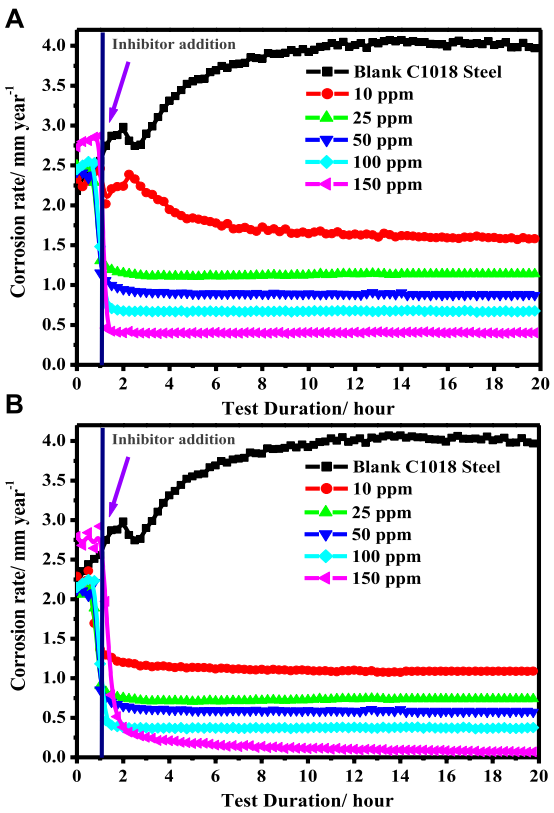


**FIGURE 6 |** Change of the corrosion rate with immersion time for C-steel in blank 3.5% NaCl saturated with carbon dioxide and inhibited medium containing a different concentrations of **(A)** CSM and **(B)** CSD at 50 ± 1°C.

surfactants in $CO_2$-saturated 3.5% brine solution and the *n* value enhanced considerably, demonstrating respectable hindrance in contradiction of sweet corrosion and the products of corrosion process movement from the metal surface.

Generally, when a corrosion additive is inserted into a corrosive solution, the $C_{dl}$ values will turn lesser, and this infers that the constant of local dielectric declines and/or double-layer thickness increases, supporting the C-steel corrosion protection by the surfactant adsorption at the interface of C-steel/$CO_2$-saturated 3.5% NaCl (Hsissou et al., 2020c).

The double-layer thickness is the reciprocal of capacitance and could be utilized to follow the inhibitor species adsorption process on the metal interface. For instance, for CSM and CSD surfactants (150 mg $L^{-1}$), the capacitance ($C_{dl}$) value (197.70 μF $cm^{-2}$) attained for the blank system is reduced to 31.71 μF $cm^{-2}$ for CSM and 23.42 μF $cm^{-2}$ for CSD, indicating that the CSD surfactant performs as a respectable capacitance reducer and consequently a superior corrosion additive. Furthermore, a decline in $C_{dl}$ with cumulative surfactant dose was detected which might be ascribed to the development of a defensive film by the surfactant additive adsorption at the C-steel/brine solution interface (Shahzad et al., 2020).

**Figures 5I,II** show the Bode and phase angle modules at different doses of the studied surfactant additives. As observed from **Figure 5**, Bode profiles denote the presence of a sole constant phase component at the interface of C-steel/$CO_2$-saturated brine. At low frequencies, the impedance values are augmented owing to the construction of the protection layer by the surfactant molecule adsorption, which shields C-steel from harsh ions. The extreme phase-angle at the middle frequency for a perfect capacitor is −90°. In the lack of CSM and CSD surfactants, the value of the phase angle is lesser than the values detected in the inhibited medium. The increase in maximum phase-angle with an upsurge in the surfactant dose confirms the adsorption of more surfactant molecules on the metal interface (Singh et al., 2019), resulting in a reduction in the dissolution rate of the metal. Additionally, more phase-angle values are detected in the case of CSD, which clarifies its superior inhibition characteristics. In the pre-eminent condition, the protection efficacy value of about 92.6 and 96.1% was obtained in the presence of 150 ppm of CSM and CSD, respectively, after 45 min metal exposure to the corrosive medium.

## Effect of Dipping Time (Stability of the Surfactant)

The LPR corrosion rate was performed to confirm the stability of the extracted natural surfactants in the titled corrosive medium. **Figures 6A,B** show the change of the rate of (CR) corrosion with dipping time for C-steel in blank brine solution saturated with carbon dioxide and inhibited medium containing different concentrations of (A) CSM and (B) CSD at 50 ± 1 °C. The CSM and CSD surfactant additives were introduced into the 3.5% NaCl saturated with carbon dioxide after 1 hour of dipping (at this period, $E_{cor}$ becomes stable). In the blank corrosive medium, the CR was augmented with *t* from 2.354 to 3.969 mm/y after 20 hours of immersion, that is, the CR inclines to upsurge with exposure time in the blank corrosion system. This behavior could be recognized to the galvanic impact among $Fe_3C$ (cementite) and α-Fe (ferrite phase) (Abd El-Lateef et al., 2020). From **Figures 6A,B**, a sharp decline in the *CR* was distinguished after the insertion of CSM and CSD surfactants to the 3.5% NaCl saturated with carbon dioxide as a corrosive solution. The CR was decreased from 3.969 mm/y to 0.401 and 0.068 mm/y by the addition of 150 ppm of CSM and CSD, respectively, after 20 h of dipping. These phenomena might be attributed to the adsorption of CSM and CSD molecules and the construction of a nature-protecting layer at the electrode/electrolyte interface; consequently, the metal interface is regularly isolated from the corrosive environments (Tantawy et al., 2020). It is observed from **Figures 6A,B** that the CR values declined, while the protection capacity enhanced with cumulative (CSM and CSD) and extends to the highest value of 89.9 and 98.2% in the presence of 150 ppm of CSM and CSD, respectively, after 20 h of dipping. The increased protection capacity upon increasing [surfactant] is ascribed to an upsurge in the part of the covered surface of the CSM and CSD molecules. The findings accomplished from the LPR corrosion rate technique were established to have a suitable agreement with the data attained from the EIS and PDP methods.

It is well accepted that the inhibition efficacy of inhibitor additives is motivated by immersion during the time in the aggressive medium. So, to examine the influence of immersion time on the corrosion protection of C-steel under sweet conditions in the presence of different concentrations of (CSM and CSD) surfactants, the LPR corrosion rate method was utilized. It is observed from **Figures 6A,B** that the values of CR for C-steel in the inhibited systems containing surfactants (at all concentrations) continue from 2 to 20 h when compared with those achieved for the blank system. Nevertheless, from 2 to 20 h of soaking, the values of the corrosion rate remain steady, which may be attributed to the development of a strong surfactant layer on the steel interface which inhibits the corrosive attack of sweet corrosion on the C-steel substrate.

## Adsorption Isotherm and Corrosion Mitigation Mechanism

Actually, the $H_2O$ molecules might adsorb at the interface of the electrode/electrolyte. Consequently, the surfactant adsorption from the aqueous medium could be reflected as a quasi-replacement route among the surfactant molecules in the aqueous solution [$Sur_{(sol)}$] and $H_2O$ molecules at the metal substrate [$H_2O_{(ads)}$] as the following equation (Farelas and Ramirez, 2010).

$$Sur_{(sol)} + nH_2O_{(ads)} \leftrightarrow Sur_{(ads)} + nH_2O_{(ads)}, \quad (8)$$

where $n$ represents the number of $H_2O$ molecules substituted by one surfactant additive. Basic knowledge of the surfactant adsorption steel interface could be delivered by adsorption isotherm considerations (Singh et al., 2017). The degree of corrosion protection depends on the surface situations and adsorption approach of organic additives. Supposing that the corrosion on the surface-protected parts equalize zero and that the corrosion occurs merely on the exposed parts of the interface, the part of surface coverage is computed from **Eq. 3**. Some models of adsorption isotherms could be utilized to measure the adsorption mode of the prepared surfactants on the steel interface (Hsissou et al., 2020d; Hsissou et al., 2021b):

Temkin model

$$\exp(f\theta) = K_{ads}C_{inh}, \quad (9)$$

Langmuir model

$$\frac{\theta}{1-\theta} = K_{ads}C_{inh}, \quad (10)$$

Frumkin model

$$\frac{\theta}{1-\theta}\exp(-2f\theta) = K_{ads}C_{inh}, \quad (11)$$

Freundlich model

$$\theta = K_{ads}C_{inh}, \quad (12)$$

where $f$ represents the active factor in homogeneity, $C_{inh}$ signifies the surfactant dose, and $K_{ads}$ denotes the adsorption equilibrium constant (Hsissou et al., 2020d).

In order to obtain the best explanation of the adsorption performance of the prepared surfactants, all of the previous adsorption isotherm models were verified. The $C/\theta$ vs. $C_{inh}$ profile produced a straight line with a correlation coefficient ($R^2$) of 0.9974 and 0.9997 and a slope of 0.936 and 0.948 for CSM and CSD, respectively, as presented in **Figure 7**. This indicates that the adsorption of the surfactant on the electrode interface follows the model of Langmuir isotherm. On the other hand, the value of $K_{ads}$ could be intended from the straight-line intercept of the $C/\theta$ vs. $C_{inh}$ curve, and the associated standard free energy of adsorption ($\Delta G^0_{ads}$) could be expressed by the subsequent equation (Li et al., 1999):

$$\Delta G^0_{ads} = -2.303RT\log(1 \times 10^6 K_{ads}), \quad (13)$$

where the value of $1 \times 10^6$ is ($H_2O$), $R$ is the general gas-constant, and $T$ is Kelvin temperature.

The calculated $K_{ads}$ values were found to be 62.6 and 91.7 L $g^{-1}$ and $\Delta G^0_{ads}$ are −48.2 and −49.3 kJ $g^{-1}$ for CSM and CSD, respectively. The high $K_{ads}$ value shows that the surfactant molecule owns strong adsorption capability onto the steel interface, and the negative $\Delta G^0_{ads}$ values show that the surfactants are instinctively adsorbed on the electrode surface (Ouici et al., 2017). Normally, $\Delta G^0_{ads}$ values close to −20 kJ $g^{-1}$ or lesser are reliable with the electrostatic attraction among charged surfactant molecules and charged steel substrates (physical adsorption); while those close to −40 kJ $g^{-1}$ or greater include transfer from the surfactant additive molecule to the steel substrate to form covalent bonds (chemical adsorption)

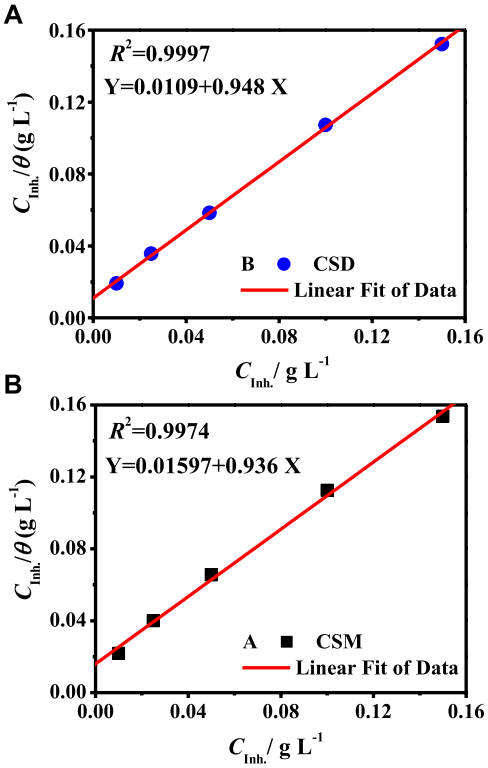


**FIGURE 7 |** $C/\theta$ vs. $C_{inh}$ profile derived from Langmuir isotherm model for C-steel in 3.5% NaCl saturated with carbon dioxide at 50 ± 1°C.

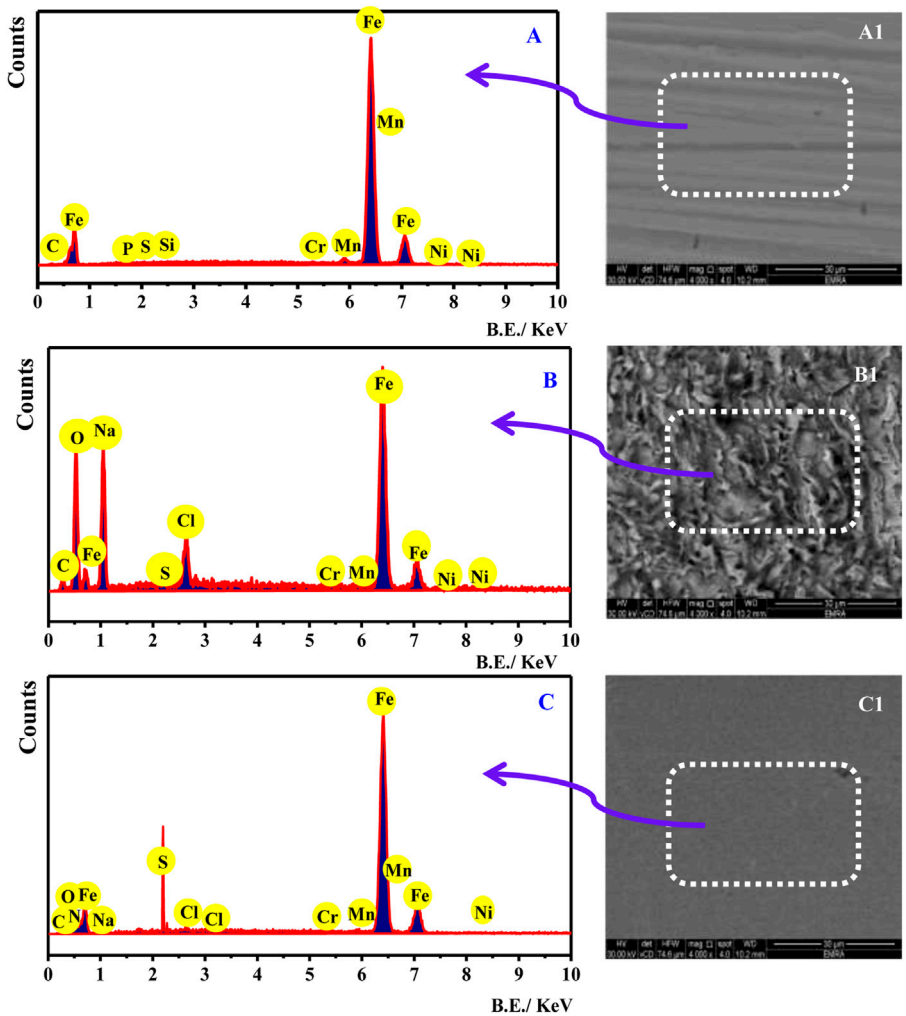


**FIGURE 8 |** EDX analysis **(A–C)** and FESEM **(A1–C1)** micrograph of **(A)** pristine C-steel, **(B)** C-steel immersed in blank 3.5% NaCl saturated with $CO_2$, and **(C)** C-steel immersed in 3.5% NaCl saturated with $CO_2$ containing 150 ppm CSD for 20 h.

(Usman et al., 2017). In this study, the $\Delta G^0_{ads}$ values are more than −40.0 kJ $g^{-1}$, demonstrating that the prepared natural surfactants are chemically adsorbed on the metal substrate.

Surfactant molecule adsorption takes place due to the attraction energy between the surfactant species and the electrode substrate, which is greater than that between $H_2O$ molecules and the electrode substrate. Subsequently, the mitigation impact by surfactants is related to the robust surfactant adsorption *via* their active sites onto the electrode substrate. Herein, the findings show that the mechanism of adsorption of the tested surfactants on metal in brine solution saturated with $CO_2$ is characteristic of chemisorption at the experiment temperature. Chemical adsorption of the surfactant additive could happen owing to the construction of links among the empty d-orbital of Fe atoms, including the $H_2O$ molecule displacement from the steel substrate and the lone pairs of electrons existing on the nitrogen, sulfur, and/or oxygen atoms of the surfactant. The rate of the adsorption process is commonly quick and, therefore, the reactive steel is isolated from the corrosive medium (Shalabi et al., 2019). Moreover, there is a synergism between $Cl^-$ ion adsorption and the protonated surfactant molecules. In addition, the adsorbed surfactant species could be combined with the oxide film and react chemically to produce an additional protecting surface system (Cai et al., 2013; Migahed et al., 2018). Consequently, we could conclude that the corrosion inhibition of CSM and CSD in brine solution saturated with $CO_2$ is mostly owing to electrostatic and chemical attractions.

## Comparative Study of Some Designated Corrosion Additives for C-Steel Under Sweet Conditions

**Supplementary Table S2** (Supporting data) shows the comparison of the inhibition activity of the synthesized natural surfactants based on soybean oil (CSM and CSD) for

the corrosion of C-steel alloy under the sweet condition ($CO_2$-saturated 3.5% NaCl) with some previously designated surfactant additives (Farelas and Ramirez, 2010; Singh et al., 2017; Singh et al., 2019; Shahzad et al., 2020; Hsissou et al., 2021b). The inhibition capacity values, recorded in **Supplementary Table S2**, were acquired utilizing EIS, LPR corrosion rate, and PDP experiments. By comparing these outcomes, it was found that our natural surfactants (CSM and CSD) are the pre-eminent effective inhibitors in 3.5% NaCl saturated with $CO_2$. Likewise, the highest inhibition capacity value is attained using a 150 ppm concentration of CSD, that is, 98.6%.

## Surface Characteristics by EDX/FESEM and XPS

The FESEM complemented with the EDX system was used to confirm the adsorption of the surfactant molecule at the electrode/electrolyte interface. **Figure 8** shows the EDX analysis (A, B, and C) and FESEM (A1, B1, and C1) micrograph of (A) pristine C-steel, (B) C-steel immersed in blank 3.5% NaCl saturated with $CO_2$, and (C) C-steel immersed in 3.5% NaCl saturated with $CO_2$ containing 150 ppm CSD for 20 h. **Figure 8A** displays EDX analysis for C-steel substrate. The feature peaks are due to (Fe, Cr, C, P, S, Si, and Mn) elements existing in the alloy structure. **Figure 8A1** illustrates the picture of the pristine C-steel surface. The image shows the metal surface brightness lacking any presence. After immersion in the corrosive medium without the inhibitor (**Figure 8B**), the surface reveals that the feature peaks are due to Mn, P, Fe, Cr, and O elements. This designated that the products of corrosion process on the C-steel substrate creature metal oxides. The corresponding picture (**Figure 8B1**) exhibited a dense spongy film of corrosion product enclosing all the metal substrates, revealing that in the uninhibited medium, the electrode interface is extremely corroded. However, in the inhibited corrosive medium containing 150 ppm of CSD (**Figure 8C**), the surfactant displays extra characteristic peaks of nitrogen element. This outcome demonstrated that the surfactant adsorption on the C-steel substrate leads to decline in the corrosion film, and a greater dose of the surfactant is essential to interval the corrosion process, while the SEM picture in the inhibited system (**Figure 8C1**) shows a smooth surface, which determines a respectable defensive layer existing on the C-steel substrate. These findings support the PDP and EIS measurements.

The XPS investigations were accompanied to verify the CSD surfactant adsorption on the electrode substrate. The XPS exploration attained for C1018-steel in blank brine solution saturated with $CO_2$ solution (A–D) and the occurrence of 150 mg/L CSD (E-J) are presented in **Supplementary Figure S3**. The communal bands for Fe-2p, Cl-2p, C-1s, and O-1s were identified for the protected and unprotected sample. Furthermore, the peaks of S-2p and N-1s were detected for the C1018-steel sample dipped in the solutions containing the inhibitor, which approves the CSD surfactant adsorption on a metal interface.

For the blank medium, the profile of C-1s indicates three peaks (**Supplementary Figure S3A**) at 288.5, 287.2, and 285.3 eV might be labeled to –C=O/$COOO^-$, –C–O/$COOO^{-}$,and–-C–C–, respectively, whereas the protected sample at 284.6 might be ascribed to the C–H and–-C–C– bonds, 286.4 could be recognized to –C–S and –C–N bonds, and 288.6 eV can be related to $^+$N–C– bond (Ouici et al., 2017). The occurrence of Cl band (**Supplementary Figures S3B,F**) on the metal interface in the picked sample lacking and with the CSD surfactant in 3.5% NaCl solutions saturated with carbon dioxide could be ascribed to the attraction between the $Cl^-$ ions and the surface positive charge of metal generating iron (III) chloride (Bouanis et al., 2016). The Cl-2p band exposes two peaks for the blank and protected sample which is due to Cl-$2p_{3/2}$ at 197.9 and 197.8 and Cl-$2p_{1/2}$ at 199.9 and 199.5 eV, respectively (Bouanis et al., 2016).

The XPS profile of iron-2p indicates that four bands (**Supplementary Figures S3C,G**) for the blank and protected sample at 709.9 and 710.1 eV is given for Fe-$2p_{3/2}$ of Fe(II), where 712.9 and 712.8 eV is related to Fe-$2p_{3/2}$ of Fe(III), 718.4, 720.2; 724.3, and 723.6 and 729.5 and 731.4 eV are attributed to Fe-$2p_{3/2}$, Fe-$2p_{1/2}$, and Fe-$2p_{1/2}$, respectively (Hashim et al., 2019). In addition, the O-1s profile possesses three bands (**Supplementary Figures S3D,I**) for the blank and protected C1018-steel sample which might be related to O atoms, $CO_3^-$, and $OH^-$ bonded to Fe(II) and Fe(III) to form the FeO/$Fe_2O_3$ oxides, $FeCO_3$, and FeOOH, respectively (Cen et al., 2019).

Furthermore, the metal electrode in the corrosive medium containing the CSD surfactant displays additional peaks for N-1s and S-2p spectra exposing one band (**Supplementary Figures S3H,J**) at 398.9 and 167.5 eV which might be ascribed to the –N–H and –$SO_3^-$ existing in the CSD compound, respectively. According to the XPS outcomes, we could confirm that the CSD surfactant is adsorbed at the interface of steel/solution.

## DFT Calculations

The optimized geometry of the synthesized natural surfactants CSM and CSD at the B3LYP level of theory and their HOMO and LUMO orbital occupation are presented in **Figure 9**. The binding of surfactant species to the C-steel interface increases with a greater energy value of HOMO, which specifies the superior electron donation of the surfactant molecule to the empty d-orbital of the steel, and a lesser energy level of LUMO denotes the capability of the surfactant additive to gain electrons from the d-orbital of steel (Abdallah et al., 2018). As recorded in **Table 3**, if we compare among the surfactants, CSD has a greater HOMO and lesser LUMO energy value that demonstrates that CSD displays greater protection capacity than the CSM surfactant additive. The adsorption capability of the surfactant increases with lesser energy gap ($\Delta E$). The lesser energy gap states greater chemical reactivity and protection efficiency (Gece and Bilgiç, 2009). The tendency for $\Delta E$ values has the order CSM > CSD or $CSMH^+$> $CSDH^+$ (**Table 3**). These outcomes demonstrate that the protonated forms have larger inclination to adsorb on the steel interface than the non-protonated forms.

For the two models, the HOMO and LUMO as seen in **Figure 9** are generally localized at the terminal edges of the

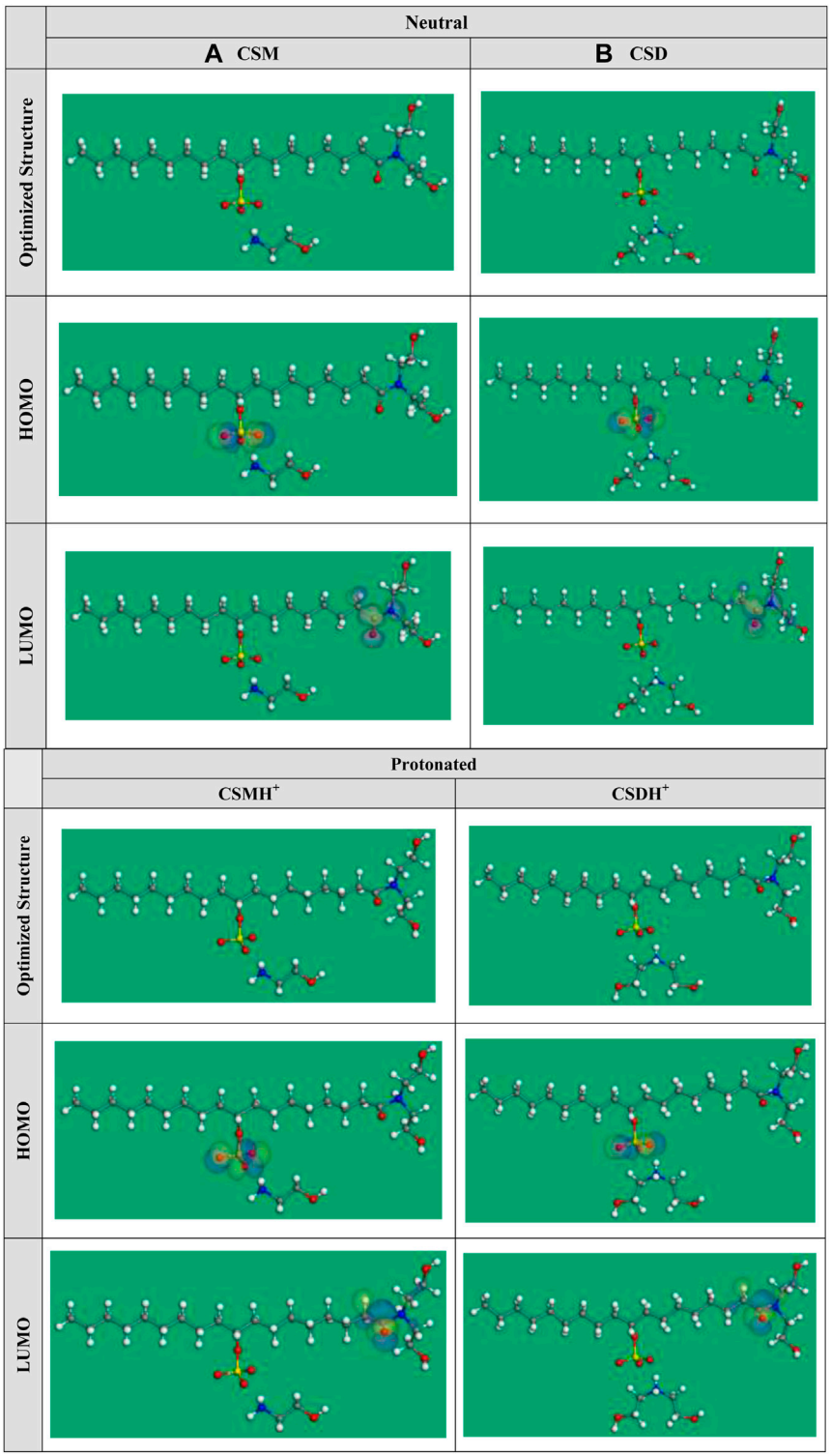


**FIGURE 9 |** Optimized structure and HOMO and LUMO orbital occupation for the investigated **(A)** CSM and **(B)** CSD surfactants in neutral and protonated forms.

surfactant molecule, where the cationic part chains are placed. The dipole moment ($\mu$) is a significant theoretical parameter that reveals the global polarity of a surfactant molecule. The μ is associated with protection power. The protection capacity increases with increasing the $\mu$. As revealed in **Table 3**, the CSD and $CSDH^+$ forms have the maximum $\mu$.

**TABLE 3 |** DFT parameters of the protonated and neutral CSM and CSD surfactants.

| Parameter | Non-protonated form | | Protonated form | |
|---|---|---|---|---|
| | CSM | CSD | $CSMH^+$ | $CSDH^+$ |
| $E_{HOMO}$ (eV) | −5.43 | −5.45 | −5.50 | −5.51 |
| $E_{LUMO}$ (eV) | −0.38 | −0.60 | −2.78 | −2.86 |
| $\Delta E = E_{LUMO} - E_{HOMO}$ (eV) | 5.05 | 4.85 | 2.72 | 2.65 |
| Electronegativity ($\chi$) | 2.91 | 3.03 | 4.14 | 4.19 |
| Global hardness ($\eta$) | 2.53 | 2.42 | 1.36 | 1.33 |
| Global softness ($\sigma$) | 0.40 | 0.41 | 0.73 | 0.75 |
| Global electrophilicity index ($\omega$) | 1.67 | 1.90 | 6.30 | 6.60 |
| Dipole moments ($\mu$) Debye | 22.99 | 34.25 | 59.57 | 66.32 |
| Number of electrons transferred ($\Delta N$) | 0.81 | 0.82 | 1.05 | 1.06 |
| $\Delta E_{back\text{-}donation}$ | −0.63 | −0.61 | −0.34 | −0.33 |

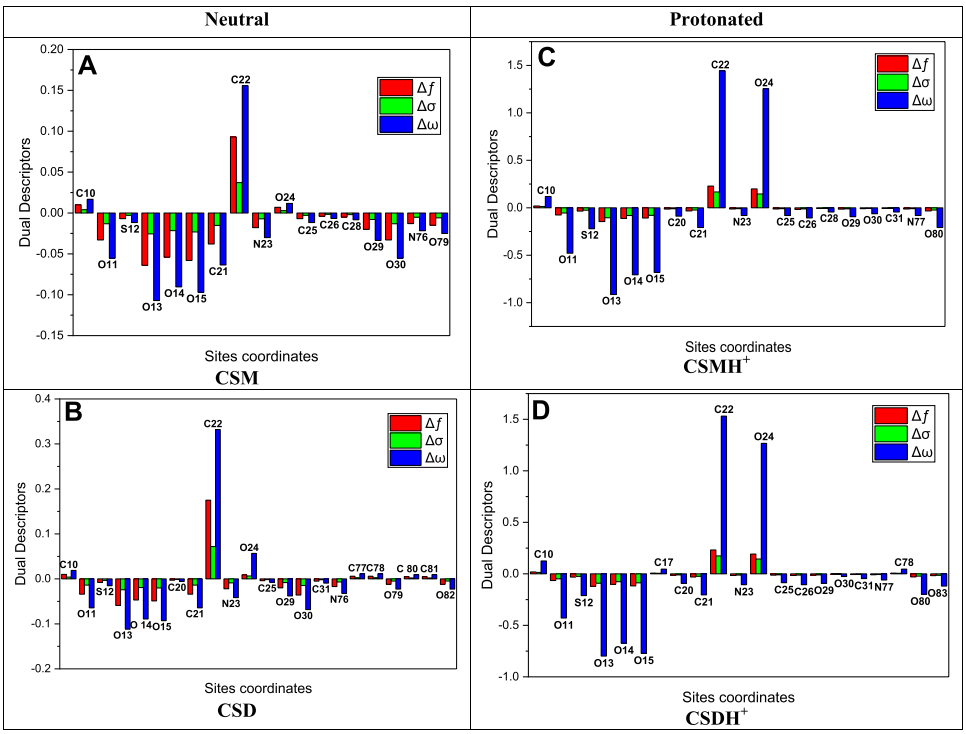


**FIGURE 10 |** Graphical representation of the dual descriptors ($\Delta f$, $\Delta\sigma$, and $\Delta\omega$) for the most active sites of the investigated CSM and CSD surfactants in neutral **(A,B)** and protonated **(C,D)** forms using the DFT method.

Global hardness ($\eta$) and softness ($\sigma$) for the two CSM and CSD compounds were intended, which estimate the surfactant molecule reactivity. The compound which has greater softness value and lesser hardness value is predicted to have the highest protection efficiency. As a result, as detected in **Table 1**, the CSD inhibitor displays higher protection power than the CSM surfactant molecule.

The local reactivity of the synthesized surfactants molecules could be assessed by computing the Fukui indices ($f_k^+$ and $f_k^-$), local softness descriptor ($\sigma_k^{\pm}$), and the local electrophilicity ($\omega_k^{\pm}$) and the dual descriptors ($\Delta f_k, \Delta\sigma_k$ and $\Delta\omega_k$) as follows (Hsissou et al., 2021b):

$$\sigma_k^{\pm} = \sigma f_k^{\pm}. \tag{14}$$

$$\omega_k^{\pm} = \omega f_k^{\pm}. \tag{15}$$

$$\Delta f_k^{\pm} = f_k^+ - f_k^-. \tag{16}$$

$$\Delta\sigma_k = \sigma_k^+ - \sigma_k^-. \tag{17}$$

$$\Delta\omega_k = \omega_k^+ - \omega_k^-. \tag{18}$$

For simplifying, the most important findings are exhibited in **Supplementary Table S3**. The calculated Fukui indices (**Supplementary Table S3**) support the electron distribution of the HOMO and LUMO orbitals detected for the neutral and protonated species assigning the sites; thus, the synthesized surfactants will be adsorbed onto the metal surface. $f_k^-$ represents the reactivity of the electrophilic attack (donation

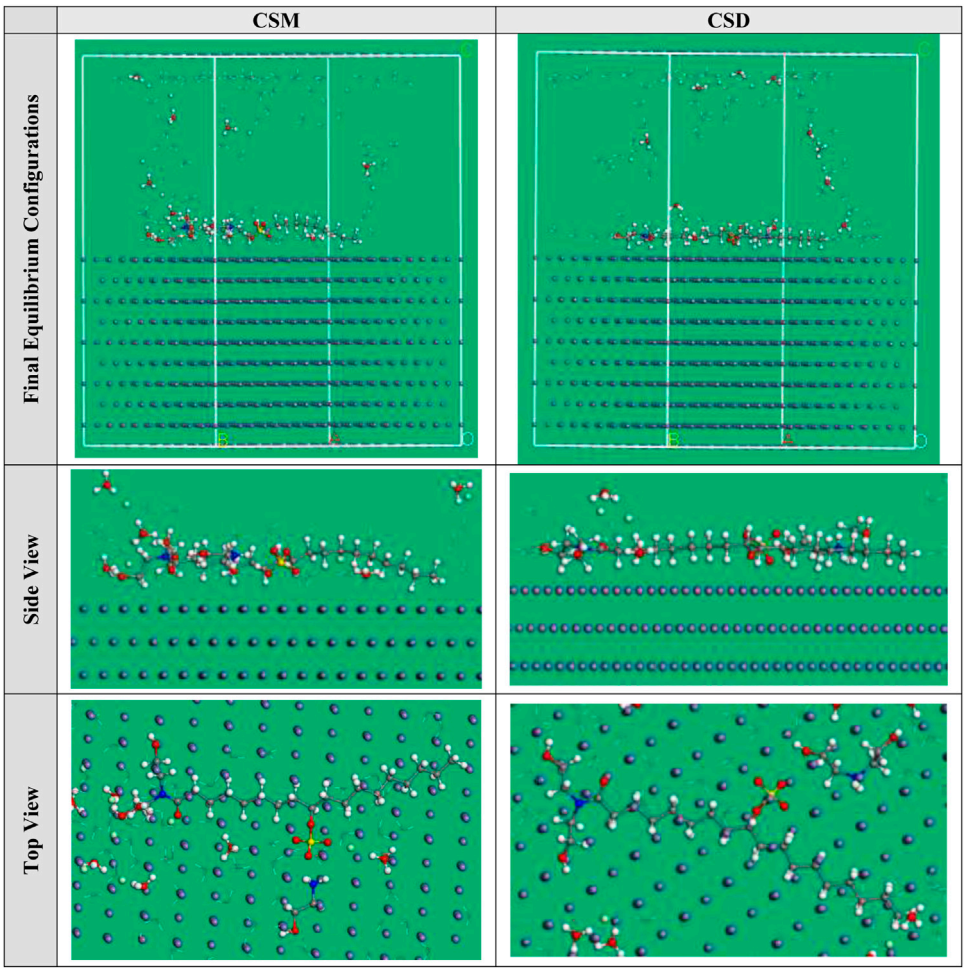


**FIGURE 11 |** Most suitable adsorption configuration for the structure of **(A)** CSM and **(B)** CSD surfactants on Fe (1 1 0) substrate obtained by the adsorption locator module.

sites), whereas $f_k^+$ signifies the reactivity of the nucleophilic attack (accepting centers) (Hsissou, 2021). The highest $f_k^-$ for the neutral form of the synthesized surfactants is found at O11, S12, O13–O15, C22, N23, O24, and O30 and the protonated form at O11, S12, O13–O15, C22, N23, O24, O29, O30, and O80, designating the site for offering electrons, whereas the highest $f_k^+$ is found at S12, C22, N23, O24, and O30 for the neutral form and at O11, O13–O15, O24, O29, and O30 for the protonated form, exhibiting back-donation capability (Hsissou et al., 2021c). Moreover, the local dual descriptors are more accurate and reliable tools than the Fukui indices ($f_k^+$ and $f_k^-$), and local softness ($\sigma_k^{\pm}$) and electrophilicity ($\omega_k^{\pm}$) and the graphical representation of the dual local descriptors of the maximum descriptive active sites are demonstrated in **Figure 10**. The obtained findings disclose that the sites with the $\Delta f_k, \Delta\sigma_k$, and $\Delta\omega_k < 0$ have the affinity to contribute electrons to the metal surface. In contrast, those centers with $\Delta f_k, \Delta\sigma_k$, and $\Delta\omega_k > 0$ have the capability to receive electrons from the metal. It is obvious that in **Figure 10**, the greatest active sites for electron contribution are at O11, S12, O13–O15, C21, N23, C25–C28, O29, O30, N76, and O79 for the neutral form and O11, S12, O13–O15, C20, C21, N23, O24, C25–C28, O29, O30, C31, N77, and O80 for the protonated form, while the active accepting centers are at C10, C22, and O24 for both neutral and protonated forms.

The electron transferred number ($\Delta N$) is also computed and recorded in **Table 3**. If the $\Delta N$ values ˂ 3.6, the protection capacity upsurges by increasing the capability of surfactant molecules to contribute electrons to the C-steel interface (Obot et al., 2016). As observed in **Table 3**, the values of $\Delta N$ for the prepared natural surfactants are positive, and the CSD displays a greater value than CSM additive, which provides a suggestion that CSD additive has greater protection capacity more than the CSM compound.

From the outcomes in **Table 3** the $\Delta N$ values are in the order [$CSDH^+$ (1.06)> $CSMH^+$ (1.05)> CSD (0.82)> CSM (0.81)]. Herein, CSM and CSD surfactants are the electron donors, and the metal interface is the acceptor. This outcome supports the fact that the CSM and CSD adsorption on the metal substrate can happen by donor–acceptor attractions among π-electrons and/or nonbonding lone pair electrons of the N- atom and empty

**TABLE 4 |** Data and descriptors calculated by the Monte Carlo simulation (MC) for the adsorption of the structure CSM and CSD surfactants on Fe (1 1 0).

| Corrosion system | Adsorption energy/ kcal $mol^{-1}$ | Rigid adsorption energy/kcal $mol^{-1}$ | Deformation energy/ kcal $mol^{-1}$ | $dE_{ads}/dN_i$: inhibitor | $dE_{ads}/dN_i$: $Cl^-$ ions (kcal $mol^{-1}$) | $dE_{ads}/dN_i$: hydronium (kcal $mol^{-1}$) | $dE_{ads}/dN_i$: water (kcal $mol^{-1}$) |
|---|---|---|---|---|---|---|---|
| Fe (110) CSM Water Hydronium $Cl^-$ ions | −2700.14 | −2874.08 | 173.94 | −165.54 | −95.79 | −43.48 | −13.06 |
| Fe (110) CSD Water Hydronium $Cl^-$ ions | −2836.76 | −3012.51 | 175.75 | −242.56 | −97.61 | −46.22 | −13.97 |

d-orbitals of Fe. Based on the previous computational indices, it could be recognized that the protonated $CSMH^+$ and $CSDH^+$ forms are more efficient than neutral CSM and CSD forms.

## MC Simulations

MC simulations were performed to acquire more information about the interaction between the iron surface and surfactant molecule (El-Lateef et al., 2019). We have confirmed that the full system touched equilibrium until both energy and temperature were composed. The equilibrium shape (top, side views, and final equilibrium configurations) of the Fe(110)/$Cl^-$/surfactant/$H_2O$ adsorption model is depicted in **Figure 11**. **Figure 11** reveals the greatest suitable adsorption arrangements for the CSM and CSD molecules on the Fe (1 1 0) surface, which are signified in approximately parallel or flat arrangement, and the surfactant compound is adsorbed on the steel interface *via* nitrogen atom (N), demonstrating an improvement in the magnitude of adsorption and maximum surface coverage (Madkour et al., 2018). Furthermore, the directories assessed from MC simulations are listed in **Table 4**. As per **Table 4**, the CSD molecule has high negative adsorption energy (−2836.76 kcal $mol^{-1}$) than that for the CSM molecule (−2700.14 kcal $mol^{-1}$), which designates that the adsorption of the CSD molecule on the Fe(110) interface is strong, spontaneous, and stable. This indicated that when the corrosive ions, such as $Cl^-$ ions and $H_2O$ molecules, exist at the surface, the inhibitive CSM and CSD molecules could approach the steel interface accordingly, suggesting their tendency for interfacial attachment to the metal adsorbent (Özcan et al., 2004). Moreover, the CSD molecule in the investigated corrosive medium provides higher rigid adsorption energy (−3012.51 kcal $mol^{-1}$) than the CSM (−2874.08 kcal $mol^{-1}$) molecule, which indicates that the CSD molecule will adsorb more powerfully on the steel interface and possess excellent protection capacity.

The $dE_{ads}/dN_i$ is the adsorption energy if one of the adsorbates was eliminated (Zhang et al., 2020). The $dE_{ads}/dN_i$ values for hydronium ions, water molecules, and $Cl^-$ ions are smaller than the values of the CSM and CSD molecules, suggesting that the strong adsorption of the CSM and CSD is higher than that of water molecules, hydronium ions, and $Cl^-$ ions. So, this proves the exchange of the other species by the CSM and CSD molecules. Therefore, the CSM and CSD molecules are resolutely adsorbed on the steel surface and produce a robust adsorbed defensive film resulting in the protection for the C-steel substrate in the studied aggressive medium, which is confirmed by experiential and DFT investigations together.

## CONCLUSION

In the current study, the protective effect of two natural surfactants based on soybean oil was inspected *via* different morphological (XPS and FESEM/EDX) and electrochemical (PDP, LPR corrosion rate) examinations and combined with DFT calculations and MC simulations. The diverse experimental methods were in good agreement, presenting that CSD is a superior inhibitor compared to CSM under the same conditions, and the protection capacities augmented with the increase in the surfactant dose, reaching the maximum values 97.6 and 98.6% in the presence of 150 ppm of CSM and CSD, respectively. Also, the PDP profiles showed that the prepared natural surfactants could control the corrosion process by a mixed-type mechanism. The steel corrosion process was inhibited by the adsorption of CSM and CSD on the metallic interface, and their adsorption follows Langmuir model. The formation of protective film was confirmed by FESEM/EDX and XPS methods. The stability of surfactants in the studied corrosive medium (sweet conditions) was confirmed by the LPR corrosion rate until 20 h. Alongside experimental investigations, the DFT calculations revealed that the efficient electron-rich areas of surfactant species are the main centers in their adsorption. MD simulations reveal that the presence of nitrogen atoms (N) in CSM and CSD structure plays an important role in the adsorption route. In consonance with the empirical finding, the theoretical outcomes displayed that the sequence of protection capacity was CSD > CSM.

## DATA AVAILABILITY STATEMENT

The original contributions presented in the study are included in the article/**Supplementary Material**; further inquiries can be directed to the corresponding authors.

## AUTHOR CONTRIBUTIONS

HAE-L contributed to conceptualization, supervision, investigation, methodology, resources, formal analysis, data curation, funding acquisition, writing—original draft, and writing—review and editing. HE-B helped with resources, funding acquisition, writing—original draft, and writing—review and editing. MM assissted with resources, funding acquisition, writing—original draft, and writing—review and editing. MKa was responsible for resources, formal analysis, writing—original draft, and writing—review and editing. AT involved in writing—original draft and writing—review and editing. EB: investigation, methodology, formal analysis, data curation, writing—original draft, and writing—review and editing. KS contributed to investigation, methodology, formal analysis, data curation, writing—original draft, and writing—review and editing. MKh helped with investigation, methodology, formal analysis, data curation, writing—original draft, and writing—review and editing.

## ACKNOWLEDGMENTS

The authors extend their appreciation to the Deputyship for Research and Innovation, Ministry of Education of Saudi Arabia, for funding this research work through the project number IFT20203.

## SUPPLEMENTARY MATERIAL

The Supplementary Material for this article can be found online at: https://www.frontiersin.org/articles/10.3389/fmats.2022.843438/full#supplementary-material

## REFERENCES

Abd El-Lateef, H. M. (2020). Corrosion Inhibition Characteristics of a Novel Salycilidene Isatin Hydrazine Sodium Sulfonate on Carbon Steel in HCl and a Synergistic Nickel Ions Additive: A Combined Experimental and Theoretical Perspective. *Appl. Surf. Sci.* 501, 144237. doi:10.1016/j.apsusc.2019.144237

Abd El-Lateef, H. M., Shalabi, K., and Tantawy, A. H. (2020). Corrosion Inhibition and Adsorption Features of Novel Bioactive Cationic Surfactants Bearing Benzenesulphonamide on C1018-Steel under Sweet Conditions: Combined Modeling and Experimental Approaches. *J. Mol. Liquids* 320, 114564. doi:10.1016/j.molliq.2020.114564

Abd El-Lateef, H. M., and Tantawy, A. H. (2016). Synthesis and Evaluation of Novel Series of Schiff Base Cationic Surfactants as Corrosion Inhibitors for Carbon Steel in Acidic/chloride media: Experimental and Theoretical Investigations. *RSC Adv.* 6, 8681–8700. doi:10.1039/c5ra21626e

Abdallah, Y. M., Shalabi, K., and Bayoumy, N. M. (2018). Eco-friendly Synthesis, Biological Activity and Evaluation of Some New Pyridopyrimidinone Derivatives as Corrosion Inhibitors for API 5L X52 Carbon Steel in 5% Sulfamic Acid Medium. *J. Mol. Struct.* 1171, 658–671. doi:10.1016/j.molstruc.2018.06.045

Alnajjar, A. O., Abd El-Lateef, H. M., Khalaf, M. M., and Mohamed, I. M. A. (2022). Steel protection in Acidified 3.5% NaCl by Novel Hybrid Composite of $CoCrO_3$/polyaniline: Chemical Fabrication, Physicochemical Properties, and Corrosion Inhibition Performance. *Construction Building Mater.* 317, 125918. doi:10.1016/j.conbuildmat.2021.125918

Ansari, K. R., Quraishi, M. A., and Singh, A. (2014). Schiff's Base of Pyridyl Substituted Triazoles as New and Effective Corrosion Inhibitors for Mild Steel in Hydrochloric Acid Solution. *Corrosion Sci.* 79, 5–15. doi:10.1016/j.corsci.2013.10.009

Bentiss, F., Lebrini, M., and Lagrenée, M. (2005). Thermodynamic Characterization of Metal Dissolution and Inhibitor Adsorption Processes in Mild Steel/2,5-Bis(n-Thienyl)-1,3,4-Thiadiazoles/hydrochloric Acid System. *Corrosion Sci.* 47, 2915–2931. doi:10.1016/j.corsci.2005.05.034

Bouanis, M., Tourabi, M., Nyassi, A., Zarrouk, A., Jama, C., and Bentiss, F. (2016). Corrosion Inhibition Performance of 2,5-Bis(4-Dimethylaminophenyl)-1,3,4-Oxadiazole for Carbon Steel in HCl Solution: Gravimetric, Electrochemical and XPS Studies. *Appl. Surf. Sci.* 389, 952–966. doi:10.1016/j.apsusc.2016.07.115

Cai, B., Dong, J., Cheng, L., Jiang, Z., Yang, Y., and Li, X. (2013). Adsorption and Micellization of Gemini Surfactants with Pyrrolidinium Head Groups: Effect of the Spacer Length. *Soft Matter* 9, 7637. doi:10.1039/c3sm50916h

Cen, H., Cao, J., Chen, Z., and Guo, X. (2019). 2-Mercaptobenzothiazole as a Corrosion Inhibitor for Carbon Steel in Supercritical CO2-H2O Condition. *Appl. Surf. Sci.* 476, 422–434. doi:10.1016/j.apsusc.2019.01.113

Chen, S., Singh, A., Wang, Y., Liu, W., Deng, K., and Lin, Y. (2017). Inhibition Effect of Ilex Kudingcha C.J. Tseng (Kudingcha) Extract on J55 Steel in 3.5wt% NaCl Solution Saturated with $CO_2$. *Int. J. Electrochem. Sci.* 12, 782–796.

Clemente, T. E., and Cahoon, E. B. (2009). Soybean Oil: Genetic Approaches for Modification of Functionality and Total Content. *Plant Physiol.* 151, 1030–1040. doi:10.1104/pp.109.146282

Desimone, M. P., Grundmeier, G., Gordillo, G., and Simison, S. N. (2011). Amphiphilic Amido-Amine as an Effective Corrosion Inhibitor for Mild Steel Exposed to CO2 Saturated Solution: Polarization, EIS and PM-IRRAS Studies. *Electrochimica Acta* 56, 2990–2998. doi:10.1016/j.electacta.2011.01.009

El-Lateef, H. M. A., Abdallah, Z. A., and Ahmed, M. S. M. (2019). Solvent-free Synthesis and Corrosion Inhibition Performance of Ethyl 2-(1,2,3,6-Tetrahydro-6-Oxo-2-Thioxopyrimidin-4-Yl)ethanoate on Carbon Steel in Pickling Acids: Experimental, Quantum Chemical and Monte Carlo Simulation Studies. *J. Mol. Liquids* 296, 111800–111815. doi:10.1016/j.molliq.2019.111800

Farelas, F., and Ramirez, A. (2010). Carbon Dioxide Corrosion Inhibition of Carbon Steels through Bis-Imidazoline and Imidazoline Compounds Studied by EIS. *Int. J. Electrochem. Sci.* 5, 797–814.

García, M. T., Campos, E., Sanchez-Leal, J., and Ribosa, I. (1999). Effect of the Alkyl Chain Length on the Anaerobic Biodegradability and Toxicity of Quaternary Ammonium Based Surfactants. *Chemosphere* 38, 3473–3483. doi:10.1016/s0045-6535(98)00576-1

Gece, G., and Bilgiç, S. (2009). Quantum Chemical Study of Some Cyclic Nitrogen Compounds as Corrosion Inhibitors of Steel in NaCl media. *Corrosion Sci.* 51, 1876–1878. doi:10.1016/j.corsci.2009.04.003

Haque, J., Ansari, K. R., Srivastava, V., Quraishi, M. A., and Obot, I. B. (2017). Pyrimidine Derivatives as Novel Acidizing Corrosion Inhibitors for N80 Steel Useful for Petroleum Industry: A Combined Experimental and Theoretical Approach. *J. Ind. Eng. Chem.* 49, 176–188. doi:10.1016/j.jiec.2017.01.025

Hashim, N. Z. N., Anouar, E. H., Kassim, K., Zaki, H. M., Alharthi, A. I., and Embong, Z. (2019). XPS and DFT Investigations of Corrosion Inhibition of Substituted Benzylidene Schiff Bases on Mild Steel in Hydrochloric Acid. *Appl. Surf. Sci.* 476, 861–877. doi:10.1016/j.apsusc.2019.01.149

Hsissou, R., Abbout, S., Benhiba, F., Seghiri, R., Safi, Z., Kaya, S., et al. (2021c). Insight into the Corrosion Inhibition of Novel Macromolecular Epoxy Resin as Highly Efficient Inhibitor for Carbon Steel in Acidic Mediums: Synthesis, Characterization, Electrochemical Techniques, AFM/UV-Visible and Computational Investigations. *J. Mol. Liquids* 337, 116492. doi:10.1016/j.molliq.2021.116492

Hsissou, R., Abbout, S., Berisha, A., Berradi, M., Assouag, M., Hajjaji, N., et al. (2019b). Experimental, DFT and Molecular Dynamics Simulation on the Inhibition Performance of the DGDCBA Epoxy Polymer against the Corrosion of the E24 Carbon Steel in 1.0 M HCl Solution. *J. Mol. Struct.* 1182, 340–351. doi:10.1016/j.molstruc.2018.12.030

Hsissou, R., Abbout, S., Safi, Z., Benhiba, F., Wazzan, N., Guo, L., et al. (2021b). Synthesis and Anticorrosive Properties of Epoxy Polymer for CS in [1 M] HCl Solution: Electrochemical, AFM, DFT and MD Simulations. *Construction Building Mater.* 270, 121454. doi:10.1016/j.conbuildmat.2020.121454

Hsissou, R., Abbout, S., Seghiri, R., Rehioui, M., Berisha, A., Erramli, H., et al. (2020d). Evaluation of Corrosion Inhibition Performance of Phosphorus Polymer for Carbon Steel in [1 M] HCl: Computational Studies (DFT, MC and MD Simulations). *J. Mater. Res. Techn.* 9, 2691–2703. doi:10.1016/j.jmrt.2020.01.002

Hsissou, R., Benhiba, F., Abbout, S., Dagdag, O., Benkhaya, S., Berisha, A., et al. (2020b). Trifunctional Epoxy Polymer as Corrosion Inhibition Material for Carbon Steel in 1.0 M HCl: MD Simulations, DFT and Complexation Computations. *Inorg. Chem. Commun.* 115, 107858. doi:10.1016/j.inoche.2020.107858

Hsissou, R., Benhiba, F., Dagdag, O., El Bouchti, M., Nouneh, K., Assouag, M., et al. (2020c). Development and Potential Performance of Prepolymer in Corrosion Inhibition for Carbon Steel in 1.0 M HCl: Outlooks from Experimental and Computational Investigations. *J. Colloid Interf. Sci.* 574, 43–60. doi:10.1016/j.jcis.2020.04.022

Hsissou, R., Benhiba, F., Echihi, S., Benkhaya, S., Hilali, M., Berishae, A., et al. (2021a). New Epoxy Composite Polymers as a Potential Anticorrosive Coatings for Carbon Steel in 3.5% NaCl Solution: Experimental and Computational Approaches. *Chem. Data Collections* 31, 100619. doi:10.1016/j.cdc.2020.100619

Hsissou, R., Benzidia, B., Rehioui, M., Berradi, M., Berisha, A., Assouag, M., et al. (2020). Anticorrosive Property of Hexafunctional Epoxy Polymer HGTMDAE for E24 Carbon Steel Corrosion in 1.0 M HCl: Gravimetric, Electrochemical, Surface Morphology and Molecular Dynamic Simulations. *Polym. Bull.* 77, 3577–3601. doi:10.1007/s00289-019-02934-5

Hsissou, R., Dagdag, O., Abbout, S., Benhiba, F., Berradi, M., El Bouchti, M., et al. (2019a). Novel Derivative Epoxy Resin TGETET as a Corrosion Inhibition of E24 Carbon Steel in 1.0 M HCl Solution. Experimental and Computational (DFT and MD Simulations) Methods. *J. Mol. Liquids* 284, 182–192. doi:10.1016/j.molliq.2019.03.180

Hsissou, R., and Elharfi, A. (2020). Rheological Behavior of Three Polymers and Their Hybrid Composites (TGEEBA/MDA/PN), (HGEMDA/MDA/PN) and (NGHPBAE/MDA/PN). *J. King Saud Univ. - Sci.* 32, 235–244. doi:10.1016/j.jksus.2018.04.030

Hsissou, R. (2021). Review on Epoxy Polymers and its Composites as a Potential Anticorrosive Coatings for Carbon Steel in 3.5% NaCl Solution: Computational Approaches. *J. Mol. Liq.* 336, 116307. doi:10.1016/j.molliq.2021.116307

Hua, Y., Barker, R., and Neville, A. (2015). Comparison of Corrosion Behaviour for X-65 Carbon Steel in Supercritical CO2-saturated Water and Water-Saturated/unsaturated Supercritical CO2. *J. Supercrit. Fluids* 97, 224–237. doi:10.1016/j.supflu.2014.12.005

Juárez, E. G., Mena-Cervantes, V. Y., Vazquez-Arenas, J., Flores, G. P., and Hernandez-Altamirano, R. (2018). Inhibition of CO2 Corrosion via Sustainable Geminal Zwitterionic Compounds: Effect of the Length of the Hydrocarbon Chain from Amines. *ACS Sustain. Chem. Eng.* 6 (12), 17230–17238. doi:10.1021/acssuschemeng.8b04619

Kowsari, E., Payami, M., Amini, R., Ramezanzadeh, B., and Javanbakht, M. (2014). Task-specific Ionic Liquid as a New green Inhibitor of Mild Steel Corrosion. *Appl. Surf. Sci.* 289, 478–486. doi:10.1016/j.apsusc.2013.11.017

Li, S. L., Wang, Y. G., Chen, S. H., Yu, R., Lei, S. B., Ma, H. Y., et al. (1999). Some Aspects of Quantum Chemical Calculations for the Study of Schiff Base Corrosion Inhibitors on Copper in NaCl Solutions. *Corrosion Sci.* 41, 1769–1782. doi:10.1016/s0010-938x(99)00014-1

Li, S., Zeng, Z., Harris, M. A., Sánchez, L. J., and Cong, H. (2019). CO2 Corrosion of Low Carbon Steel under the Joint Effects of Time-Temperature-Salt Concentration. *Front. Mater.* 6, 10. doi:10.3389/fmats.2019.00010

Liu, X., Okafor, P. C., and Zheng, Y. G. (2009). The Inhibition of CO2 Corrosion of N80 Mild Steel in Single Liquid Phase and Liquid/particle Two-phase Flow by Aminoethyl Imidazoline Derivatives. *Corrosion Sci.* 51, 744–751. doi:10.1016/j.corsci.2008.12.024

Madkour, L. H., Kaya, S., and Obot, I. B. (2018). Computational, Monte Carlo Simulation and Experimental Studies of Some Arylazotriazoles (AATR) and Their Copper Complexes in Corrosion Inhibition Process. *J. Mol. Liquids* 260, 351–374. doi:10.1016/j.molliq.2018.01.055

Migahed, M. A., Al-Sabagh, A. M., Zaki, E. G., Mostafa, H. A., and Fouda, A. S. (2014). Synthesis of Some Novel Cationic Surfactants and Evaluation of Their Performance as Corrosion Inhibitors for X-65 Type Carbon Steel under $H_2S$ Environment. *Int. J. Electrochem. Sci.* 9, 7693–7711.

Migahed, M. A., elgendyelgendy, A., El-Rabiei, M. M., Nady, H., and Zaki, E. G. (2018). Novel Gemini Cationic Surfactants as Anti-corrosion for X-65 Steel Dissolution in Oilfield Produced Water under Sweet Conditions: Combined Experimental and Computational Investigationsfield Produced Water under Sweet Conditions: Combined Experimental and Computational Investigations. *J. Mol. Struct.* 1159, 10–22. doi:10.1016/j.molstruc.2018.01.033

Musa, A. Y., Kadhum, A. A. H., Mohamad, A. B., and Takriff, M. S. (2011). Molecular Dynamics and Quantum Chemical Calculation Studies on 4,4-Dimethyl-3-Thiosemicarbazide as Corrosion Inhibitor in 2.5M H2SO4. *Mater. Chem. Phys.* 129, 660–665. doi:10.1016/j.matchemphys.2011.05.010

Nesõić, S. (2007). Key Issues Related to Modelling of Internal Corrosion of Oil and Gas Pipelines a Review. *Corrosion Sci.* 49, 4308–4338.

Obot, I. B., Kaya, S., Kaya, C., and Tüzün, B. (2016). Density Functional Theory (DFT) Modeling and Monte Carlo Simulation Assessment of Inhibition Performance of Some Carbohydrazide Schiff Bases for Steel Corrosion. *Physica E: Low-dimensional Syst. Nanostructures* 80, 82–90. doi:10.1016/j.physe.2016.01.024

Olajire, A. A. (2017). Corrosion Inhibition of Offshore Oil and Gas Production Facilities Using Organic Compound Inhibitors - A Review. *J. Mol. Liquids* 248, 775–808. doi:10.1016/j.molliq.2017.10.097

Ortega-Toledo, D. M., Gonzalez-Rodriguez, J. G., Casales, M., Martinez, L., and Martinez-Villafañe, A. (2011). CO2 Corrosion Inhibition of X-120 Pipeline Steel by a Modified Imidazoline under Flow Conditions. *Corrosion Sci.* 53, 3780–3787. doi:10.1016/j.corsci.2011.07.028

Ouici, H., Tourabi, M., Benali, O., Selles, C., Jama, C., Zarrouk, A., et al. (2017). Adsorption and Corrosion Inhibition Properties of 5-amino 1,3,4-Thiadiazole-2-Thiol on the Mild Steel in Hydrochloric Acid Medium: Thermodynamic, Surface and Electrochemical Studies. *J. Electroanalytical Chem.* 803, 125–134. doi:10.1016/j.jelechem.2017.09.018

Özcan, M., Dehri, İ., and Erbil, M. (2004). Organic sulphur-containing Compounds as Corrosion Inhibitors for Mild Steel in Acidic media: Correlation between Inhibition Efficiency and Chemical Structure. *Appl. Surf. Sci.* 236, 155–164. doi:10.1016/j.apsusc.2004.04.017

Ramírez-Estrada, Al., Mena-Cervantes, V. Y., Elizalde, I., Manzo-Robledo, A., Zamudio-Rivera, O. S., Nieto-Álvarez, D. A., et al. (2017). Development of a Zwitterionic Compound Derived from β-Amino Acid as a Green Inhibitor for $CO_2$ Corrosive Environments. *ACS Sustain. Chem. Eng.* 5, 1110396–1110406. doi:10.1021/acssuschemeng.7b02434

Saha, S. K., Ghosh, P., Hens, A., Murmu, N. C., and Banerjee, P. (2015). Density Functional Theory and Molecular Dynamics Simulation Study on Corrosion Inhibition Performance of Mild Steel by Mercapto-Quinoline Schiff Base Corrosion Inhibitor. *Physica E: Low-dimensional Syst. nanostructures* 66, 332–341. doi:10.1016/j.physe.2014.10.035

Saleh, M. M., Mahmoud, M. G., and Abd El-Lateef, H. M. (2019). Comparative Study of Synergistic Inhibition of Mild Steel and Pure Iron by 1-hexadecylpyridinium Chloride and Bromide Ions. *Corrosion Sci.* 154, 70–79. doi:10.1016/j.corsci.2019.03.048

Shahzad, K., Sliem, M. H., Shakoor, R. A., Radwan, A. B., Kahraman, R., Umer, M. A., et al. (2020). Electrochemical and Thermodynamic Study on the Corrosion Performance of API X120 Steel in 3.5% NaCl Solution. *Sci. Rep.* 10, 4314. doi:10.1038/s41598-020-61139-3

Shalabi, K., and AhmedNazeer, A. (2019). Ethoxylates Nonionic Surfactants as Promising Environmentally Safe Inhibitors for Corrosion protection of Reinforcing Steel in 3.5 % NaCl Saturated with $Ca(OH)_2$ Solution. *J. Mol. Struct.* 1195, 863–876.

Shalabi, K., Helmy, A. M., El-Askalany, A. H., and Shahba, M. M. (2019). New Pyridinium Bromide Mono-Cationic Surfactant as Corrosion Inhibitor for Carbon Steel during Chemical Cleaning: Experimental and Theoretical Studies. *J. Mol. Liquids* 293, 111480–111494. doi:10.1016/j.molliq.2019.111480

Shapaval, V., Afseth, N., Vogt, G., and Kohler, A. (2014). Fourier Transform Infrared Spectroscopy for the Prediction of Fatty Acid Profiles in Mucor Fungi Grown in media with Different Carbon Sources. *Microb. Cel Fact.* 13, 86. doi:10.1186/1475-2859-13-86

Singh, A., Ansari, K. R., Haque, J., Dohare, P., Lgaz, H., Salghi, R., et al. (2018). Effect of Electron Donating Functional Groups on Corrosion Inhibition of Mild Steel in Hydrochloric Acid: Experimental and Quantum Chemical Study. *J. Taiwan Inst. Chem. Eng.* 82, 233–251. doi:10.1016/j.jtice.2017.09.021

Singh, A., Ansari, K. R., Quraishi, M. A., Kaya, S., and Banerjee, P. (2019). The Effect of an N-Heterocyclic Compound on Corrosion Inhibition of J55 Steel in Sweet Corrosive Medium. *New J. Chem.* 43, 6303–6313. doi:10.1039/c9nj00356h

Singh, A., Ansari, K. R., Quraishi, M. A., Lgaz, H., and Lin, Y. (2018). Synthesis and Investigation of Pyran Derivatives as Acidizing Corrosion Inhibitors for N80 Steel in Hydrochloric Acid: Theoretical and Experimental Approaches. *J. Alloys Comp.* 762, 347–362. doi:10.1016/j.jallcom.2018.05.236

Singh, A., Lin, Y.-h., Zhu, C.-y., Wu, Y.-p., and Ebenso, E. E. (2015). Use of HPHT Autoclave to Determine Corrosion Inhibition Effect of Poly(methyl Methacrylate-Co-N-Vinyl-2-Pyrrolidone) on Carbon Steels in 3.5% NaCl Solution Saturated with $CO_2$. *Chin. J. Polym. Sci.* 33, 339–348. doi:10.1007/s10118-015-1587-1

Singh, A., Talha, M., Xu, X., Sun, Z., and Lin, Y. (2017). Heterocyclic Corrosion Inhibitors for J55 Steel in a Sweet Corrosive Medium. *ACS Omega* 2, 8177–8186. doi:10.1021/acsomega.7b01376

Singh, D. K., Kumar, S., Udayabhanu, G., and John, R. P. (2016). 4(N,N-dimethylamino) Benzaldehyde Nicotinic Hydrazone as Corrosion Inhibitor for Mild Steel in 1 M HCl Solution: An Experimental and Theoretical Study. *J. Mol. Liquids* 216, 738–746. doi:10.1016/j.molliq.2016.02.012

Soltani, N., Salavati, H., Rasouli, N., Paziresh, M., and Moghadas, A. (2016). Adsorption Andcorrosion Inhibition Effect of Schiff Base Ligands on Low Carbon Steel Corrosion in Hydrochloric Acid Solution. *Chem. Eng. Commun.* 203, 840–854. doi:10.1080/00986445.2015.1076801

Tantawy, A. H., Soliman, K. A., and Abd El-Lateef, H. M. (2020). Novel Synthesized Cationic Surfactants Based on Natural Piper Nigrum as Sustainable-green Inhibitors for Steel Pipeline Corrosion in $CO_2$-3.5% NaCl: DFT, Monte Carlo Simulations and Experimental Approaches. *J. Clean. Prod.* 250, 119510. doi:10.1016/j.jclepro.2019.119510

Usman, J., Umoren, S. A., and Gasem, Z. M. (2017). Inhibition of API 5L X60 Steel Corrosion in $CO_2$-saturated 3.5% NaCl Solution by Tannic Acid and Synergistic Effect of KI Additive. *J. Mol. Liquid* 237, 146–156. doi:10.1016/j.molliq.2017.04.064

Yang, X., Zhang, R., Pu, J., He, Z., and Xiong, L. (2021). 2D Graphene and H-BN Layers Application in Protective Coatings. *Corros Rev.* 39 (2), 93–107. doi:10.1515/corrrev-2020-0080

Yilmaz, N., Fitoz, A., Ergun, ÿ., and Emregül, K. C. (2016). A Combined Electrochemical and Theoretical Study into the Effect of 2-((thiazole-2-Ylimino)methyl)phenol as a Corrosion Inhibitor for Mild Steel in a Highly Acidic Environment. *Corrosion Sci.* 111, 110–120. doi:10.1016/j.corsci.2016.05.002

Zhang, R., Xiong, L., He, Z., Pu, J., and Guo, L. (2021). Synthesis and Structure of Water-Soluble Sb Quantum Dots and Enhanced Corrosion Inhibition Performance and Mechanisms. *Inorg. Chem.* 60 (21), 16346–16356. doi:10.1021/acs.inorgchem.1c02172

Zhang, R., Zhu, M., Pu, J., He, Z., and Xiong, L. (2021). A New Strategy for Achieving N Modified Graphene and as Protective Coating for Cu: First-Principles Investigations. *Surf. Inter.* 24, 101048. doi:10.1016/j.surfin.2021.101048

Zhang, W., Ma, Y., Chen, L., Wang, L.-J., Wu, Y.-C., and Li, H.-J. (2020). Aloe Polysaccharide as an Eco-Friendly Corrosion Inhibitor for Mild Steel in Simulated Acidic Oilfield Water: Experimental and Theoretical Approaches. *J. Mol. Liquids* 307, 112950–211962. doi:10.1016/j.molliq.2020.112950

Zhu, M., He, Z., Guo, L., Zhang, R., Anadebe, V. C., Obot, I. B., et al. (2021). Corrosion Inhibition of Eco-Friendly Nitrogen-Doped Carbon Dots for Carbon Steel in Acidic media: Performance and Mechanism Investigation. *J. Mol. Liquids* 342, 117583. doi:10.1016/j.molliq.2021.117583

**Conflict of Interest:** The authors declare that the research was conducted in the absence of any commercial or financial relationships that could be construed as a potential conflict of interest.

**Publisher's Note:** All claims expressed in this article are solely those of the authors and do not necessarily represent those of their affiliated organizations, or those of the publisher, the editors, and the reviewers. Any product that may be evaluated in this article, or claim that may be made by its manufacturer, is not guaranteed or endorsed by the publisher.